TOWARDS DEFINING THE ENDOMEMBRANE COMPARTMENTS OPERATING IN CELLULAR EXIT OF CORONAVIRUSES
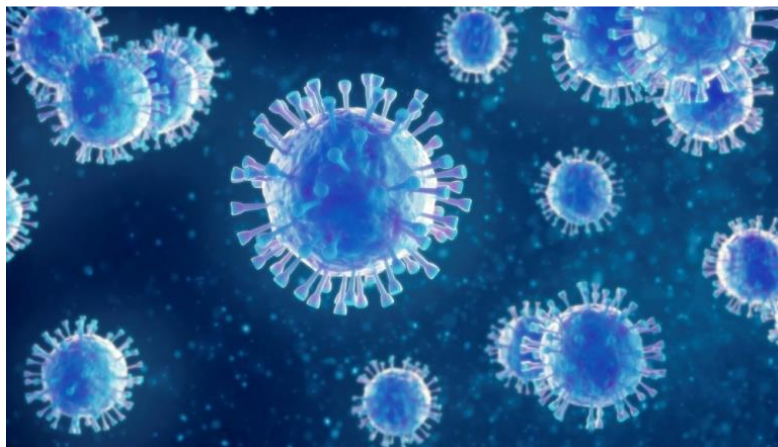
BY

MARY OZIOMA UCHE ENYIOKO

This thesis is submitted in partial fulfilment of the requirements for the degree of Master in Biomedical Sciences

Department of Biomedicine

Faculty of Medicine

University of Bergen, Norway

June 2021

ACKNOWLEDGEMENTS

TABLE OF CONTENTS

ABBREVIATIONS

ACE2	Angiotensin-converting enzyme 2
ARF	ADP ribosylation factor
CFTR	Cystic fibrosis transmembrane conductance regulator
COPI	Coat protein complex I
CoV	Coronavirus
CRD	Conserved carbohydrate recognition domain
ER	Endoplasmic reticulum
ERC	Endocytic recycling compartment
ERES	Endoplasmic reticulum exit sites
ERGIC-53	Endoplasmic reticulum intermediate compartment-protein of 53 KDa
GRASP	Golgi-reassembly and stacking protein
HA	Hemagglutinin
HCoV	Human coronavirus
HIV	Human immunodeficiency virus
IBV	Avian infectious bronchitis virus
IC	Intermediate compartment
LAMP1	Lysosomal-associated membrane protein 1
MERS-CoV	Middle east respiratory syndrome coronavirus
MHV	Mouse hepatitis virus
mRNA	messenger RNA
NA	Neuraminidase
NRK	Normal rat kidney cells
ORFs	Open reading frames
PM	Plasma membrane
PP1a/1b	Polyproteins 1a/1b
RBD	Receptor binding domain
RdRp	RNA dependent RNA polymerase

RE	Recycling endosome
Rep1a/1b	Replicase1a/1b
RNA	Ribonucleic acid
RTC	Replication transcription complexes
SARS-CoV	Severe acute respiratory syndrome coronavirus
TGN	Trans-Golgi network
TMD	Transmembrane domain
UPS	Unconventional protein secretion
VLP	Virus-like particle
vRNP	Viral ribonucleoprotein
VTC	Vesicular tubular cluster

LIST OF FIGURES

LIST OF TABLES

ABSTRACT

Coronaviruses (CoVs) are single stranded RNA viruses of positive polarity which assemble by budding into the lumen of the intermediate compartment (IC) at the endoplasmic reticulum (ER)-Golgi interface. Previously, these viruses have been mainly of veterinary interest, but since 2002 they have also been connected to serious and readily transmissible disease in humans. Therefore, particularly in light of the ongoing COVID-19 pandemic, it is important to understand the life cycle of the virus to be able to fight CoV infections. While the mechanisms of CoV entry into their host cells have been more extensively studied, the pathway(s) and mechanisms of their cellular exit remain poorly understood.

Using the avian infectious bronchitis virus (IBV) – a non-human pathogen – as a model virus the main aim of this study was to employ various microscopic techniques to obtain detailed information of the pathway(s) that CoVs follow during their delivery from the cell interior to the extracellular space. For this purpose, it was important to establish the conditions for cultivating the virus in Vero cells, determine the growth kinetics of the virus by plaque titration, as well as characterize the antibody tools available against the structural proteins of IBV. In addition, the applicability of antibodies against markers of organelles of interest (IC, *cis*-Golgi and recycling endosomes) was determined in both infected and uninfected Vero cells. Interestingly, we obtained results showing that low temperature ($31^{o}C$) can potentially be used to synchronize the release process in future experiments employing the IBV M-protein as a marker for intracellular virus particles. Finally, our preliminary findings suggest that – as reported in the case of several other RNA viruses – the pericentrosomal endocytic recycling compartment (ERC) and the GTPase Rab11 may also play key roles in cellular exit of CoVs.

1. INTRODUCTION

1.1. Viruses

Viruses can be defined as sub-light microscopic disease agents that have a parasitic intracellular life cycle. They require the machinery of a cell for their replication and thus cannot be referred to as the simplest form of life [1]. Virions are infectious virus particles which are made up of a nucleic acid genome, either deoxyribonucleic acid (DNA) or ribonucleic acid (RNA), coated with a protein shell known as the nucleocapsid and in the case of membrane viruses, an outer envelope. These coats in the virions enable the stabilization of nucleic acid which carries the information needed for virus replication and the creation of the next virus generation called progeny viruses.

The DNA or RNA genome of viruses may be either double or single stranded. The bigger the viral genome, the more complex structure they have and the more viral proteins they synthesize (see Fig.1, poxvirus). Conversely, the smaller the genome, the smaller the virus particles. For example, in the case of a simple naked virus, such as poliovirus (Fig.1), the nucleocapsid consists of a single type of capsid protein. Replication in viruses that have DNA genomes is more accurate because DNA polymerase proofreads the sequence to check for eventual errors. By contrast, the replication of viruses with RNA genomes is less accurate leading to increased mutation rate due to the lack of proofreading, since the cell recognizes RNA as a messenger molecule and not as genetic material [1].

Viruses can be defined structurally, molecularly, immunologically or clinically. Thus, they can be classified based on their biological properties, virion structure, antigenic properties, mode of replication, or genome organization. They can also be classified based on the host cells that they infect. Furthermore, animal viruses can be classified based on the strategies they employ for messenger RNA (mRNA) synthesis. Viruses that infect bacteria are known as bacteriophages, those that infect fungi are known as mycophages, while those infecting plants and animals are called plant and animal viruses, respectively. Some animal viruses can only infect a limited number of cell types, which express the right surface cell receptors to which the virions can bind, i.e. they are said to have a limited host range [2].

Viruses are polyphyletic and are likely to have multiple origins. It has been suggested that they originate from various sources, such as escaped genes from the genomes of cellular organisms,

escaped nuclei of eukaryotic cells, degenerated cells that have lost the functions needed for independent existence, or represent pre-cellular life forms. However, determining their origin is difficult because they are ancient and due to their small size, the fossil records of viruses are non-existent. Since viruses depend on their host cells for replication, there have acquired genetic elements from other sources [1].
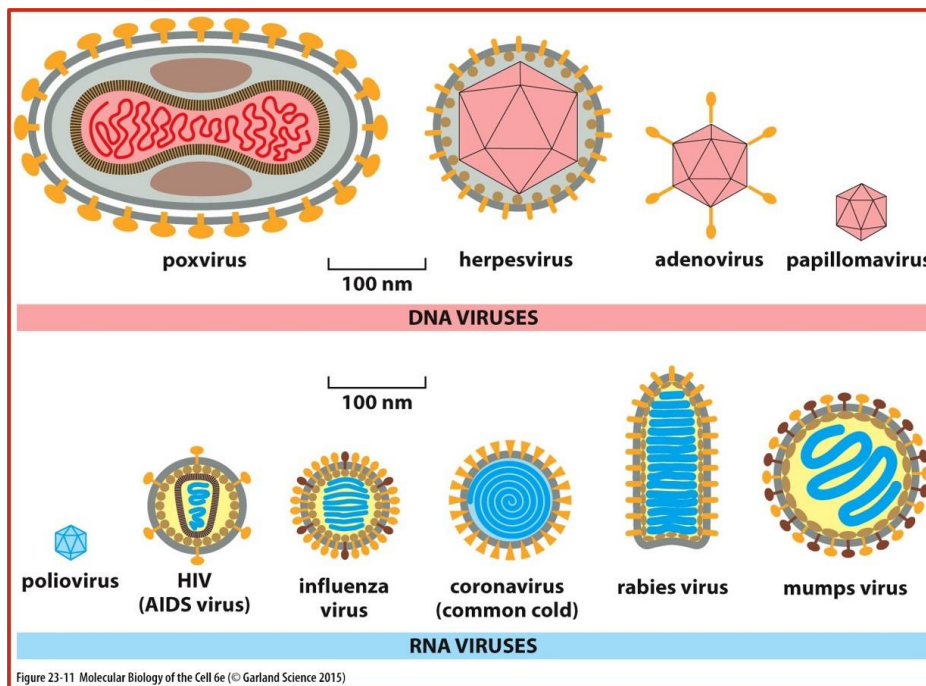
Figure 1. Examples of different DNA and RNA viruses. This figure shows schematically the structure of some naked (non-membrane) or enveloped (membrane) DNA or RNA viruses. In general, the size of the particle reflects the genomic complexity of the virus in question, as exemplified for example by poxvirus and poliovirus. However, although coronaviruses are not the largest RNA viruses in size, they have the largest known RNA genome. The figure was taken from [3].

1.2. Membrane viruses

Membrane viruses are viruses that have a viral envelope as an outermost layer to protect the genetic material. The envelope is derived from parts of the host cell's membrane which have been modified through the incorporation of virus-specific membrane glycoproteins [4]. These glycoproteins at the surface of the virion enable the virus to bind to plasma membrane (PM) receptors of the host cell. When the binding occurs, the viral envelope can fuse with the host cell membrane, enabling the virus to enter the cell and start the infection. Membrane viruses show limited survival outside their hosts, since their lipid bilayers are sensitive to detergents, heat and desiccation [5]. Membrane viruses can be classified based on their genomic composition (DNA or RNA), or structure, as shown below in Table 1.

Table 1: Selected membrane viruses and the origin of their envelopes.

Membrane virus (example viruses)	Genome	Origin of envelope
Asfarviridae (African swine fever)	DNA	ER or PM?
Hepadnaviruses (Hepatitis B)	DNA	ER or IC?
Herpesviruses (Epstein-Barr)	DNA	NE and IC/Golgi?
Poxviruses (Vaccinia)	DNA	ER, IC?
Arterivirus (Simian hemorrhagic fever)	RNA	ER
Bunyaviruses (Hantaan)	RNA	Golgi
Coronaviruses (IBV, SARS, MERS)	RNA	IC
Deltaviruses (Hepatitis D)	RNA	ER
Filoviruses (Ebola)	RNA	PM
Flaviviruses (Hepatitis C, Zika)	RNA	ER
Orthomyxoviruses (Influenza)	RNA	PM
Paramyxoviruses (Mumps, Measles)	RNA	PM
Retroviruses (HIV)	RNA	PM
Rubella virus	RNA	Golgi or PM

The table was adapted from [6]. Abbreviations: Intermediate compartment (IC), Endoplasmic reticulum (ER), Nuclear envelope (NE), Plasma membrane (PM).

1.3. Entry of membrane viruses into their host cells

The entry of membrane viruses into a host cell depends on the fusion of the viral membrane with a cellular membrane with the help of fusion proteins present at the surface of the virion. As shown in Fig. 2, specialized viral membrane proteins can act as fusogens following their activation either at the cell surface or inside the endosome [7]. Some membrane viruses have only a single protein mediating both the attachment and subsequent membrane fusion, while other viruses encode several proteins connected to these functions. The fusion needs to be precisely controlled, since it is very important for the accurate entry of the virus into the cell, resulting in the release of the genome at the right place and right time to start virus replication. Accurate fusion is also particularly

important for intracellularly budding viruses, because if the viral fusogens are prematurely activated, the viruses will fuse inside the cells and fail to be secreted.
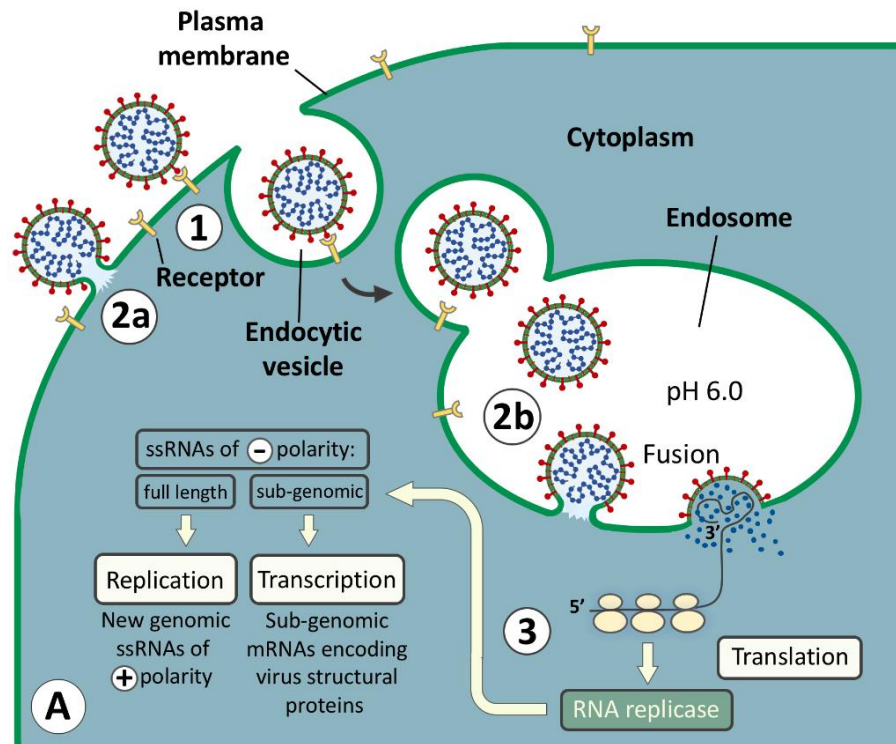
Figure 2. Entry of an enveloped RNA virus, such as a CoV, into its host cell. The virus recognizes and binds to a specific receptor at the cell surface (Step 1). This may lead to a conformational change in the receptor-binding viral protein, triggering fusion of the viral membrane with the plasma membrane (Step 2a). Alternatively, the virus is taken up by the cell via receptor-mediated endocytosis and enters endosomes, where the low lumenal pH triggers fusion between the viral and endosomal membranes (Step 2b). Subsequently, the nucleocapsid undergoes uncoating in the cytosol and the viral RNA genome is released so that its replication and transcription of the viral genes can begin (Step 3). The specific events shown here relate to CoV replication, as discussed below. The figure is from [8].

Upon activation of the fusion protein, the fusion of the viral membrane with a cellular membrane can take place either in pH-independent or -dependent manner. In the first case, the interaction of the virus with its receptor triggers a conformational change in the fusion protein, leading to fusion of the viral membrane with the PM and subsequent release of the genetic material of the virus to the cytosol (Fig. 2). In the latter case, the virus-receptor complex is internalized and transported to the endosome where the acidic lumen conditions trigger the conformational change of the viral fusion protein [9] [10]. This change allows direct interaction between the two bilayers. For example, in the case the retrovirus human immunodeficiency virus (HIV), the fusion can take place already at the cell surface. By contrast, influenza virus which employs its hemagglutinin (HA) both in virus attachment

and membrane fusion is a typical example of a virus that first enters the cell and fuses with the endosomal membrane [11].

1.4. Membrane viruses budding at the PM

Budding is a very important step in the life cycle of membrane viruses because of its role in the production of progeny viruses. Many membrane viruses are released from infected cells by maturing and budding at the PM. In case of several viruses, budding has been shown to occur at particular regions of the PM known as lipid rafts. Lipid rafts are plasma membrane domains that are highly concentrated in sphingomyelin, sphingoglycolipids and cholesterol and play an important role in transport and cellular signaling [12].

The site of viral assembly and budding is thought to be largely determined by the localization of viral membrane proteins. During the budding process, many components interact (Fig. 3). The capsid protein(s) that bind to the viral nucleic acid form the nucleocapsid, which can directly interact with the viral transmembrane or matrix proteins that line the cytoplasmic side of the PM [12] [13]. According to many studies, viral spike glycoproteins which are necessary for infectivity are integrated into the forming virions through direct contacts between their cytoplasmic domains and viral core nucleocapsid components. However, recent studies have shown that negative strand RNA viruses and retroviruses may represent exceptions to this general rule as they can bud in the absence of the spike proteins with the help of the viral core components and matrix proteins [13].

Influenza virus is one of the best characterized membrane viruses budding at the PM (Fig. 3). It has a segmented single stranded RNA genome of negative polarity, which encodes for eleven proteins, including the neuraminidase (NA) and hemagglutinin (HA) spike proteins of its envelope. Both proteins are glycosylated and delivered to the PM via the secretory pathway [12]. At the late stage of virus replication, the export of the viral ribonucleoproteins (vRNPs) from the nucleus is followed by the assembly and budding of progeny viruses at the PM of the host cell. [14]. Before the newly budded viral particles leave the PM, the sialic acid residues of glycoproteins and glycolipids in the influenza virus envelope must be cleaved and removed by the enzymatic action of NA [15]. Influenza virus assembles at lipid raft-like microdomains like other membrane viruses such as HIV, Ebola, measles and Marburg viruses [16]. The amino acid residues in the transmembrane domains of HA and NA are crucial for their raft association [17].
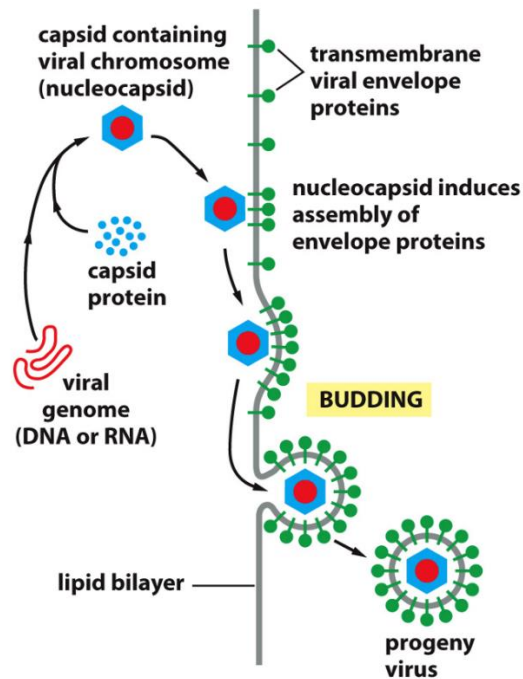
Figure 3. Budding of a membrane virus at the PM. The final assembly of many membrane viruses, such as influenza virus, takes place at the cell surface. The viral nucleocapsids, which are assembled in the cytosol from newly made viral genomes and capsid protein(s) interact with the tails of viral membrane (envelope) proteins, which have been transported to the PM. Due to this interaction the lipid bilayer bends, resulting in virus budding and release from the cell. The figure is from [3].

1.5. Membrane viruses that bud into the lumen of intracellular compartments

Although the majority of membrane viruses assemble and bud at the PM, a number of viruses are also known to bud at intracellular compartments. Their ability to form at intracellular sites stems from the fact that the viral membrane proteins mediating the budding event contain targeting information, which causes them to be retained inside the cell [18].

The intracellular compartments where these viruses assemble are usually referred to as viral factories. This is because these replication organelles shield the viruses from host defense mechanisms and make the viral replication and assembly processes more efficient [19]. The virally encoded membrane glycoproteins determine the site of viral assembly in a sub-compartment of the ER or the Golgi apparatus. The membrane viruses that assemble at intra-cellular compartments include: coronaviruses, herpesviruses, poxviruses, bunyaviruses and flaviviruses (Table 1). Some unusual events take place during the assembly of large DNA viruses, such as the passage of virions from the nucleus to the cytoplasm across the nuclear envelope, as seen in herpes viruses and, the successive envelopment by several membranes that lead to the formation of a four-membrane mature form of poxviruses [19]. The budding of

bunyaviruses into the Golgi apparatus is determined by the G1 and G2 glycoproteins of the virus, which interact with the helical viral nucleocapsids via their cytoplasmic tails. After their budding, bunyaviruses are thought to be transported along the secretory pathway from the Golgi apparatus to the extracellular space [19]. The G1 and G2 are integral membrane glycoproteins, which are generated from a common polypeptide precursor. They are both N-glycosylated during synthesis and undergo intramolecular disulfide bond formation. A number of studies indicate that the G1 protein contains the information that enables it to be retained in the Golgi, whereas the G2 protein has no retention signal and can only be retained in the Golgi when associated with G1 [20]. Furthermore, flaviviruses bud at an ER-associated compartment, which may also be related to the IC. Though the budding strategies of bunya- and flaviviruses may differ from that of CoVs, they can be expected to be released from the cell via very similar pathway [21].

According to Garoff and coworkers, the budding strategies of membrane viruses can be classified into four categories. Thus, budding can depend on both capsid and spike proteins, or is mediated only by the capsid or core protein. Furthermore, budding can depend on the viral membrane proteins only or is accomplished by a matrix protein with the help of viral membrane proteins and the ribonucleoprotein (RNP) [22]. Assembly at an intracellular compartment is advantageous for the membrane virus in the sense that the viral membrane proteins are efficiently kept within the cell, thus helping to reduce the chances that the infected cells are recognized by antibodies and killed before the production of infectious viruses takes place.

1.6. Coronaviruses (CoVs)

Coronaviruses (CoVs) are membrane viruses with a non-segmented single-stranded RNA of positive polarity, meaning that following virus entry the released RNA genome can function directly as a mRNA (see Fig. 2) [23]. They have club-like spikes projecting from their envelope giving the viruses their name. They belong to the order Nidovirales which are known to have highly conserved genomic organization, unique enzymatic activities within the replicase-transcriptase multiprotein complex and abilities to express many non-structural genes by ribosomal frameshifting and to express downstream genes by synthesis of 3′-nested sub genomic mRNAs (Fig. 2). However, members of the Nidovirus family have developed into different types of variable size or number of structural proteins [23]. They cause diseases in mammals and birds.

CoVs have the largest genome among the RNA viruses, about 30 kilobases in size. About two-thirds at the 5' end encode for two polyproteins, which give rise to the viral replicase, while about one-third at the 3' end consists of the genes for the structural proteins, as well as the accessory proteins (ORFs) [24]. CoVs possess a feature that is uncommon among positive-sense RNA viruses and in that contain helically organized nucleocapsids, which protect the RNA genome. They can mutate, recombine, and infect multiple species and cell types. The virions of CoVs are pleomorphic, showing considerable heterogeneity in their size and ranging from 100 nm to 160 nm in diameter [21]. They contain four main structural proteins namely: the spike (S) protein, a single-spanning membrane glycoprotein of approximately 150 kDa, which is heavily N-glycosylated. It mediates attachment to the host receptor and functions as a fusion protein during virus entry (Fig. 2) [25] [26]. The M protein of about 25-30 kDa is the most abundant structural protein in the virus envelope having three transmembrane domains and interacting with the other structural proteins and the genomic RNA thus giving the virion its shape. It can be modified by either addition of N-linked or O-linked sugars or in some cases both, depending on the type of CoV [21] [27].

The envelope (E) protein is a single spanning small membrane protein of about 8-12 kDa [28]. It displays ion channel activity and facilitates the assembly and release of the virus [29]. It is modified by palmitoylation and expressed abundantly in infected cells but exists only in small quantities in the virion [28]. The E protein interacts with the M protein to bring about membrane curvature during the budding process or completes virus assembly by acting as a membrane scission protein [21]. In CoV-infected cells, there are two pools of the E-protein; a monomeric pool, which interacts with a still unknown host component(s) to neutralize the luminal pH of a secretory compartment such as the Golgi apparatus. The activity of this pool supports the release of virus and as well induces disassembly of the Golgi apparatus. The second oligomeric pool of the protein participates in virus assembly [30] [31].

The nucleocapsid (N) protein is the single protein component of the CoV nucleocapsid and made up of two separate N-terminal and C-terminal domains. It uses different mechanisms to bind to the viral genome RNA in a beads-on-a-string manner [32]. Some β-CoVs contain a fifth transmembrane structural protein called the hemagglutinin-esterase (HE) which binds sialic acids on surface glycoproteins and uses its enzymatic acetyl-esterase activity to enhance S protein-mediated cell entry and virus spread through the mucosal layers of the respiratory and intestinal epithelium [33] [34].
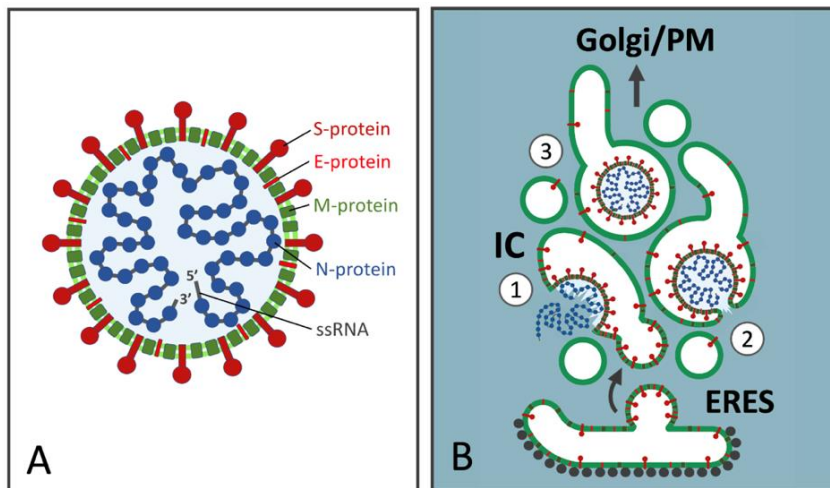
Figure 4. Structure and assembly of CoVs. (A) CoV particles consist of an envelope – a lipid bilayer (light green) containing the viral spike (S), membrane (M), envelope proteins (E). In the nucleocapsid the N protein (blue) binds in a "beads on a string" fashion from the 5ʹ to the 3ʹ end of the single-stranded viral genome RNA (ssRNA). (B) The budding of CoVs takes place at IC membranes close to ER exit sites (ERES). *Step 1*: The cytosolic nucleocapsids formed by the association of the N proteins with new viral RNA genomes, interact at the IC with the viral membrane proteins, which have been synthesized on the ER-associated ribosomes and moved to the IC in transport vesicles. *Step 2*: These interactions lead to the budding of the virus into the IC lumen. *Step 3*: The released large virus particles are now ready to move towards the PM in special transport carriers. The figure is from [21].

1.6.1. Coronavirus life cycle

The life cycle of CoVs occurs in successive stages: i) viral attachment and entry, ii) synthesis of the viral replicase, iii) genome replication and transcription, iv) synthesis of virus structural proteins, assembly, and release [23]. Mediating the attachment and entry of CoVs into their host cells, the S protein binds to a specific receptor, the angiotensin-converting enzyme 2 (ACE2), leading to its conformational change. This change enables the fusion of the viral envelope with the cell membrane already at the cell surface or following the uptake of the virus to endosomes through receptor-mediated endocytosis (see Fig. 2) [35]. Subse-quently, the genomic RNA is released into the cytosol and functions as an mRNA in the translation of polyproteins (PP1a and PP1b), which are cleaved by virus-specific enzymes (viral proteinases) into final products, leading to the production of the viral replicase (Fig. 2). The replicase then uses the positive strand genomic RNA as a template to make ssRNAs of negative polarity, which when are again transcribed to full-length new genomes or subgenomic mRNAs coding for the viral structural proteins (Fig. 2) [36] [37].

9
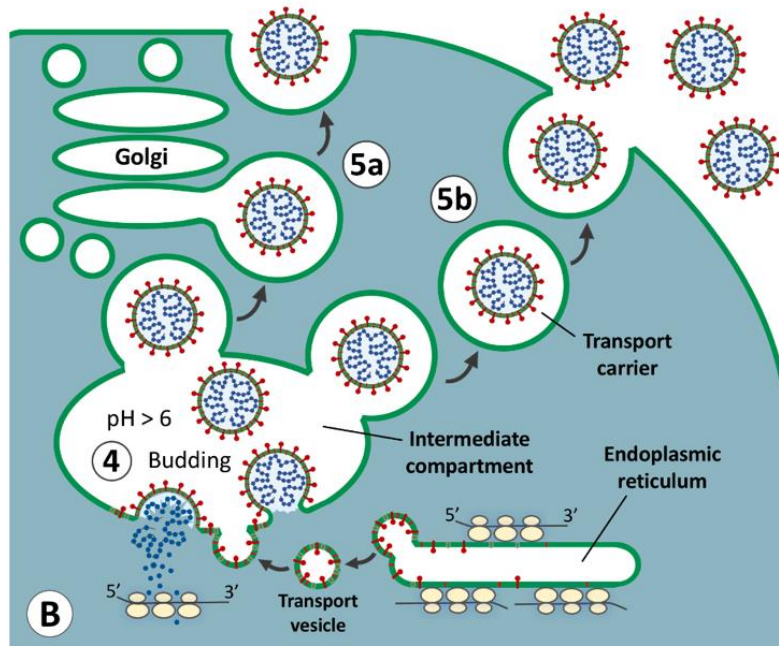
Figure 5. Release of CoVs from the infected cells. This diagram shows two possible routes for CoV exit from their host cells. Following their budding into the slightly acidic IC lumen (*Step 4*), the newly formed progeny viruses may reach the extracellular space either via a Golgi-dependent pathway (5a), or a Golgi-independent pathway (5b). This figure is derived from [8].

The viral membrane proteins (S, E and M) are translated on ER-associated ribosomes and inserted into the ER membrane. They move along the early secretory pathway to the pre-Golgi IC, where interactions between the genome RNA- and N protein-containing helical nucleocapsids and the cytoplasmic domains of the viral membrane proteins take place, resulting in virus assembly by budding into the IC lumen (Figs. 4 and 5) [37] [38]. The newly formed progeny viruses may now gain access to the extracellular space either via a Golgi-dependent pathway (Fig 5a) or a Golgi-independent pathway (Fig. 5b) [8].

Electron microscopic (EM) studies carried out by Tooze and coworkers on mouse hepatitis virus (MHV)-infected mouse fibroblasts revealed that at early times of infection the budding of new progeny viruses starts in pleomorphic smooth membrane structures at the ER-Golgi inter-face [39]. Subsequent work showed that this CoV "budding compartment" corresponds to the IC [40] [41] [42]. To understand the mechanisms that determine the intracellular budding of CoVs, Machamer and coworkers a undertook mutational analysis of the transiently expressed IBV M protein. These studies revealed the existence of a specific sequence motif in the first transmembrane segment of this multi-spanning membrane protein that dictated its efficient retention to the IC/*cis*-Golgi region [43] [44] [45].

1.6.2. Human coronaviruses

The different types of CoVs infecting various mammalian or avian species can be classified into four main subgroups: α-, β-, γ-, and δ- CoVs. The CoVs that infect humans belonging to the α- and β- CoV subgroups were first identified in the 1960s. The four CoV strains, α- CoVs human coronavirus-229E (HCoV-229E) and -NL6 (HCoV-NL6), and the β- CoVs HCoV-OC43 and HCoV-HKU frequently infect humans causing an upper respiratory tract illness known as common cold [46]. Additional CoVs infecting humans include the three recent viruses causing serious epidemic or pandemic: Middle East respiratory syndrome coronavirus (MERS-CoV), severe acute respiratory syndrome coronavirus (SARS-CoV) and the recent SARS-CoV-2 causing the pandemic coronavirus disease 2019 (Covid-19) [47].

Interestingly, these human CoVs exhibit considerable genetic variability. The site of variation for the SARS-CoV is seen at two gene loci: The S protein gene and the accessory gene ORF8. The MERS-CoV sites of variation are located at the S, ORF3 and ORF4b genes [48]. The newly discovered SARS-CoV-2 shows some differences in its S gene sequence which has three short insertions at the N-terminus and changes in four of the five residues in the receptor binding motif [49]. However, these three human CoVs are similar in structure, give similar symptoms and share a common mode of transmission [50] [33].

The SARS-CoV, a β-CoV causing severe respiratory disease was identified in Foshan China in November 2002. It caused the most severe human disease related to CoVs [51]. After the SARS epidemic was brought under control in 2003, a new CoV, the MERS-CoV was identified in 2012 in the Middle East, as indicated by its name. MERS-CoV is a CoV closely related to the *Tylonycteris* bat CoV HKU4 and *Pipistrellus* bat CoV HKU5 [52]. Originating from bats, and to be able to infect humans, it needs an intermediate host, which in the case of MERS was identified as camels, since humans rarely have contacts with bats. It has the longest duration of infection as compared to the SARS-CoV and SARS-CoV-2 and, during the early phase of its outbreak, approximately 50% death rate was recorded. MERS-CoV has the ability to recognize dipeptidyl peptidase 4 (DPP4) as its receptor at the cell surface, promoting the fusion of the viral envelope with the PM [53].

The SARS-CoV-2 is a β-CoV that causes Covid-19. It was discovered in November 2019 at Wuhan in China. As compared to the SARS-CoV and MERS-CoV, it is less deadly but the most infectious and most readily transmissible. It uses the ACE2 as its receptor but can also recognize another cell surface protein, the CD147 [54] [49]. Like MERS, it most likely

originates from bats and, when transferred to humans, its primary site of infection is the epithelial cells within the upper respiratory system. The receptor binding domain (RBD) in the S protein of the new SARS-CoV-2 has a much higher affinity to the human ACE2, explaining why it can spread more rapidly [50]. ACE2 is highly expressed in the epithelial cells of the lungs and gastrointestinal tract. However, it is also expressed in the kidney, heart, esophagus, ileum, testis, bladder and adipose tissues [55].

1.6.3. Avian infectious bronchitis virus (IBV)

IBV belongs to the γ- subgroup (genus) of CoV family and causes respiratory disease in different avian species (such as fowls) and replicates at the epithelial surfaces of non-respiratory organs, such as kidneys and gonads. Isolated in 1930, it represents the first identified CoV. IBV does not cause only respiratory diseases in birds, but also results in kidney damage and lowers egg production due to the fact that chicks affected by this virus at an early age receive permanent damage to their oviduct, preventing them from laying eggs later on [56]. This virus has proven difficult to control because many strains are distributed worldwide and mutations and recombination in the viral genome continuously give rise to new types of virus [57]. The S protein of IBV is cleaved into its amino terminal S1 subunit and carboxyl terminal S2 subunit. S1 enables the virus to attach to cells while the more conserved S2 enables membrane fusion. However, for IBV, the location of the RBD in S1 is unknown [58] [59].

1.7. An introduction to the conventional secretory pathway

The secretory pathway is employed by cells to deliver proteins and large particles (such as lipoproteins) to the extracellular environment, as well as to transport proteins and lipids to the cell surface and the different membrane organelles of the endomembrane system, such as lysosomes [60]. The organelles of the classical secretory pathway include the endoplasmic reticulum (ER), the pre-Golgi intermediate compartment (IC) and the Golgi apparatus, which are connected by vesicular trafficking [60]. In contrast to the cytosol, which is an oxidative environment, the luminal spaces of the secretory compartments have reducing conditions. This is important for the folding and post-translational modification of the various cargo proteins that follow this pathway, including soluble secretory proteins, membrane-bound PM or organelle proteins and lysosomal enzymes. To facilitate protein folding, the secretory pathway also contains luminal chaperones, which help the transported proteins to achieve their functional conformation [60].

The ER is the first organelle in the secretory pathway [61]. It is continuous with the outer nuclear membrane and consists of two membrane subdomains termed the rough and smooth ER. The rough ER is covered with ribosomes which are the sites of protein synthesis, while the smooth ER is devoid of ribosomes and functions in lipid synthesis. The proteins destined to enter the secretory pathway contain an N-terminal signal sequence, which directs the ribosomes to the rough ER. After the ribosomes have attached the rough ER, the newly made proteins enter the ER lumen or are incorporated into the ER membrane. Secretory proteins become enriched in ER-derived vesicles and subsequently transported via the IC to the Golgi apparatus to be further sorted and delivered to other cell organelles or secreted from the cell [60]. The currently prevailing cisternal progression or maturation hypothesis proposes that anterograde protein transport from *cis-* to *trans*-Golgi is based on the movement of the Golgi cisternae. To compensate for this process, COPI coated retrograde transport vesicles continuously retrieve resident Golgi proteins from later to earlier Golgi *cisternae* in the Golgi stacks. Finally, in the *trans*-Golgi network (TGN) proteins are sorted into transport vesicles that move to the PM and release their contents through exocytosis. Some secretory proteins are continuously secreted, while others are first stored inside the cell in secretory granules until the cell receives a stimulus that triggers their exocytosis [60].

1.7.1. Pre-Golgi intermediate compartment

The IC is an organelle in eukaryotic cells that mediates the communication between the ER and the Golgi apparatus and functions as an important sorting station for anterograde and retrograde trafficking in the early secretory pathway [41]. It is also referred to as the endoplasmic reticulum-Golgi intermediate compartment (ERGIC). In addition to protein sorting and trafficking at the ER-Golgi interface the IC has been recently assigned new functions related to cell signaling, autophagy and Golgi-independent trafficking [41]. Different models of the IC are presented in Fig. 6. The first model (Fig. 6, *Model a*) proposes that the IC represents a collection of transient transport intermediates that form at ER exit sites (ERES) through the fusion of ER-derived COPII-vesicles. They then move to the cell center developing Golgi-like properties and may gradually obtain a flat cisternal shape [41]. Such transformation of the IC into a *cis*-Golgi cisterna could result from alteration of its composition caused by COPI vesicle-mediated membrane recycling [62] [63]
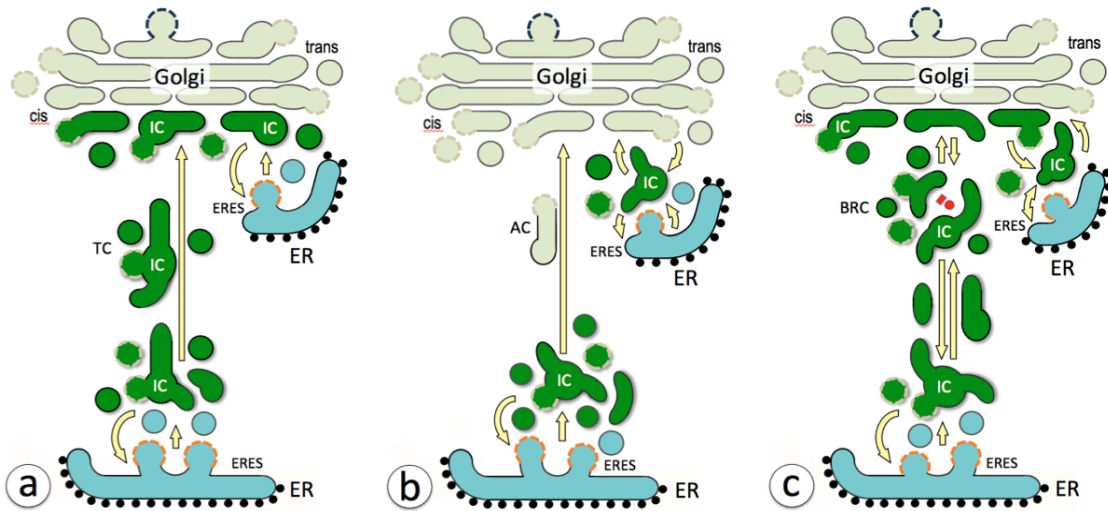
Figure 6. Different models of the IC in mammalian cells. *Model a*): The IC functions as a transient transport carrier (TC). The tubulovesicular IC elements form *de novo* at the ERES via homotypic fusion of ER-derived COPII vesicles (light blue) and fuse with or transform into Golgi elements (light green). *Model b*): A stable and immobile IC close to the ERES maintains two-way communication with the ER and the Golgi apparatus. *Model c*): According to this model the IC elements constitute a permanent membrane network, which is anchored to the centrosome (red). This model combines key aspects of the first two other models by considering that the dynamic vacuolar and tubular IC elements mediate long-distance communication within a widely distributed permanent IC system. AC = anterograde carrier. BRC = biosynthetic recycling compartment. The figure was taken from [41].

However, several studies have shown that the IC elements are not just present at the ER-Golgi boundary, but also present in the pericentrosomal region and at the cell periphery [41]. Interestingly, these widely distributed IC elements, containing the GTPase Rab1, are spatially and functionally linked to the recycling endosomes (REs) defined by the GTPase Rab1 that congregate around the centrosome [64]. Moreover, close association of these compartments is maintained when the Golgi stacks are disassembled by the drug brefeldin A (BFA), which removes membrane-bound COPI coats [65] [66]. These observations have contributed to an alternative model of the IC as a dynamic but permanent membrane system (Fig. 6, *Model c*). Together with the endocytic recycling system the IC network is proposed to function in the biogenesis of the more transient Golgi stacks, and also establish an unconventional pathway to the cell surface that is resistant to BFA, i.e. independent of the Golgi stacks [41].

The individual IC elements are often described morphologically as vesicular tubular clusters (VTCs), representing assemblies of small tubules and vesicles [67]. However, based on studies employing EM and analytical cell fractionation the IC also contains an additional saccular component of up to 0.5 µm in diameter. These large IC elements also have the ability to expand.

Since the narrow tubules and small vesicles of the VTCs lack the required luminal space to accommodate the large CoV particles, these saccular IC elements would provide a suitable IC domain where the budding of the virus can take place [40] [68]. They could also act as large-sized carriers for the transport of the newly assembled CoV particles from ERES to the central Golgi region [69].

Various molecular machineries are involved in the regulation of transport in the early secretory pathway, including cargo receptors (such as p58/ERGIC-53), Rab GTPases (such as Rab1), ADP ribosylation factors (ARFs), vesicular protein coats (COPI and COPII), tethering factors and fusion proteins [41]. Rab proteins are thought give different organelles their identity by organizing the formation of specific membrane domains through the recruitment of e.g. lipid-modifying enzymes and peripheral membrane proteins [70]. Rab1 and COPI appear to play important roles in IC organization by specifically associating with the different saccular and tubular subdomains of this organelle [41].

1.8. Unconventional protein secretion (UPS)

The conventional pathway of protein secretion, which most secretory proteins are thought to follow, involves the passage of ER-derived cargo through the Golgi apparatus. Interestingly, these is now increasing evidence showing that many proteins can be delivered to the cell surface or extracellular space in an unconventional (or non-classical) manner that is independent of the ER and/or Golgi apparatus [71]. The proteins employing such unconventional trafficking can be divided into two main categories: i) proteins containing signals for ER translocation that are transported to the cell surface in a Golgi-independent manner and ii) cytoplasmic or nuclear proteins that despite lacking an ER-translocation signal can be exported from the cell. It is important to understand these pathways because this novel mode of secretion turns out to be employed by important regulators of cell growth, differentiation, angiogenesis or immune response [71]. Examples of ER signal peptide-containing proteins that bypass the Golgi apparatus on their way to the PM include the cystic fibrosis transmembrane conductance regulator (CFTR) and Drosophila melanogaster α-integrin [72]. It has been suggested that CFTR passes via the endocytic recycling compartment during its delivery to the PM [71]. The Drosophila α-integrin again has been shown to reach the cell surface in the presence of brefeldin A (BFA), which disassembles to Golgi stacks [73].

Interestingly, the Golgi reassembly and stacking proteins (GRASPs) appear to be important players in both above described two forms of UPS [74]. These transport machinery proteins

were previously shown to be responsible for the stacked organization of the Golgi apparatus, as well as lateral linking of the stacks into a Golgi ribbon in vertebrate cells [74]. The multiple roles of the GRASPs suggest that although unconventional secretion is independent of Golgi integrity, it is nonetheless closely connected to the normal organization of the Golgi system [75] [76] [77].

2. AIMS OF THE STUDY

This master project addresses the late stages of coronavirus (CoV) life cycle. Of special interest was to obtain information on the still enigmatic pathways and mechanisms that these viruses employ during their transport from their site of budding in the pre-Golgi intermediate compartment (IC) to the extracellular space.

The specific aims were as follows:

1. To characterize organelle markers that can be used in subsequent experiments to follow the intracellular transport of CoVs.

2. To develop experimental approaches to study the release of CoVs from the infected cells using different microscopic techniques.

3. MATERIALS

Tables 2-9 list the reagents, chemicals, cell lines, antibodies, technical equipment, and disposable materials used in this study.

3.1. Basic laboratory reagents

Table 2

Reagents	Abbreviation or formula	Specifications	Source
Ammonium chloride	NH_4Cl	50 mM solution in PBS	Sigma
Di-sodium hydrogen phosphate-dihydrate	$Na_2HPO_4 - 2H_2O$		Merck
Dulbecco's phosphate buffered saline	PBS	Powder	Sigma
Ethanol	EtOH	100%	VWR
Glycerol	$C_3H_8O_3$	100%	Sigma
Guanidine-HCl	Guan-HCl	6 M solution in 50 mM Tris-buffer, pH 7.5	Sigma
Milli-Q	ddH_2O	Double-distilled water	IBM
Sodium azide	NaN_3	1000 x stock solution (20% in ddH_2O)	Sigma
Sodium dihydrogen phosphate-monohydrate	$NaH_2PO_4 - H_2O$		Merck
Sodium hydroxide	NaOH	1 M solution	Merck
Tris (hydroxymethyl)-aminomethane	Tris	0.5 M solution, pH 7.5	Merck

3.2. Reagents for cell culture

Table 3

Reagents	Abbreviation or formula	Specifications	Source
Dulbecco's Modified Eagle's Medium	DMEM (1X)	With 1g/L D-glucose, L-glutamine, sodium pyruvate	Gibco
Dulbecco's Modified Eagle's Medium	DMEM	Powder (without sodium bicarbonate)	Gibco
Fetal Calf Serum	FCS	Heat-inactivated	Gibco
HEPES buffer solution	HEPES	1 M solution, pH 7.2	Gibco
L-Glutamine, 100x	L-Glu	200mM (100 x)	Gibco
Penicillin-Streptomycin	Pen-strep	Antibiotics (100 x stock solution)	Gibco
Trypsin-Ethylenediamine-tetraacetic acid	Trypsin-EDTA	0.5% trypsin	Gibco

3.3. Reagents for immunofluorescence staining and microscopy

Table 4

Reagents	Abbreviation or formula	Specifications	Source
Blocking buffer		Washing buffer with 0.2% saponin and 5% GS (filtered)	
Bovine Serum Albumin	BSA	Fraction V	Roche
Coverslips	CVL	18 mm diameter, thickness $(0.17 \pm 0.01\text{mm})$	Chemi-Teknikk AS
Goat Serum	GS	Heat Inactivated	Gibco
Microscope objective slides			VWR
Paraformaldehyde	PFA	3% solution in 0.1 M phosphate buffer, pH 7.2	Sigma
Saponin			Sigma
Triton X-100	TX-100	10% stock solution	Pierce
Vectashield Mounting Medium		Mounting medium for fluorescence with DAPI	Vector Laboratories
Washing buffer		Washing buffer with 0.2% BSA and 0.02% azide	
Washing buffer with saponin		Washing buffer with 0.2% saponin, 0.2% BSA and 0.02% azide	

3.4. Reagents for virus infection

Table 5

Reagents	Abbreviation or formula	Specifications	Source
Crystal violet		0.05% in 20% EtOH	Sigma
Virus growth medium		DMEM with 2% FCS and Pen-Strep	
Sodium bicarbonate	$NaHCO_3$	7% solution	Sigma

3.5. Reagents for plaque titration

Table 6

Reagents	Abbreviation or formula	Specifications	Source
Agarose		1.8% in dH_2O. Analytical grade. Low EEO	Sigma
Virus growth medium (2x)	2 x medium	2 x DMEM (prepared from powder) with 4% FCS and sodium bicarbonate	

3.6. Disposables

Table 7

Materials	Specifications	Source
Centrifuge tubes	15 ml and 50 ml	Sarstedt
Culture plates	6-well plates, 25 and 75 cm^2 culture flasks	NUNC or Sarstedt
Disposable pipettes	5, 10 and 25 ml	Sarstedt
Filter paper		Whatman
Microfuge tubes	1.5ml	Sarstedt
Syringe filters	0.2µm	Millipore
Parafilm		VWR
Pasteur pipettes		VWR
pH indicator		Merck

3.7. Technical equipment used in the experiments

Table 8

Equipment	Specification	Supplier
Biosafety laminar flow hood	Holten LaminAir	Labexchange, Germany
Confocal microscope	Leica TCS SP8 STED 3X	Leica Microsystems, Germany
Fluorescence microscope	Axiovert 200M	Zeiss
IncuSafe CO_2-incubator	For virus experiments	SANYO, Japan
Light microscope	CKX31	Olympus
Milli-Q ultrapure water purification system		Millipore
Mini see-saw rocker	SSM4	STUART Scientific
Steri-cycle CO_2 incubator	For routine cell culture	Panasonic
Table-top centrifuge	Centrifuge 5415D	Eppendorf
VACUSAFE aspiration system		Integra Biosciences
Water bath	SWBD	STUART Scientific

3.8. Cell Line

Vero cells, the host cells for IBV in this study, are kidney epithelial cells derived from African Green Monkey. Originally purchased from the European Collection of Authenticated Cell Cultures (ECACC), these cells were provided to us by Yuta Ishizuka (Clive Bramham's laboratory). They can go through many cycles of division without becoming senescent. Also, unlike typical mammalian cells, they do not secrete α- or β-interferon when infected with viruses [78] and therefore can support the replication of a variety of virus types.

3.9. Virus

The model CoV used in this study is the Avian Infectious Bronchitis Virus (IBV). We obtained the original stock virus from Prof. Carolyn Machamer at the Department of Cell Biology, John's Hopkins School of Medicine (Baltimore, USA). IBV is a γ-CoV that causes respiratory and gastrointestinal disease in birds, but is harmless to humans, thus requiring only a BSL-2 facility in the laboratory. It was the first CoV that was identified and has been actively used as a model virus to study CoV replication.

3.10. Primary and secondary antibodies

Table 9a.

Primary antibodies against cellular proteins	Compartment	Source	Working dilution (IF)
Mouse anti-ERGIC-53	IC/*cis*-Golgi	Alexis	1:200 or 1:400
Mouse anti-LAMP1	Lysosome	BD Pharmingen	1:100
Mouse anti- Rab1	IC/*cis*-Golgi	Angelica Barnekow (Münster, Germany)	1:200
Mouse anti-Rab11	RE	BD Transduction labs	1:200
Mouse anti-transferrin receptor (TfR)	RE	Invitrogen	1:200
Rabbit anti-p58	IC/*cis*-Golgi	Sigma	1:200

		Bruno Goud (Paris, France), affinity purified by us	
Rabbit anti-Rab1	IC/*cis*-Golgi		1:20
Rabbit anti-Rab11 (monoclonal)	RE	Invitrogen	1:50 or 1:100
Rabbit anti-Rab11	RE	US Biologicals	1:50 or 1:100
Rabbit anti-Rab11 (polyclonal)	RE	Invitrogen	1:50

Table 9b.

Primary antibodies against IBV proteins	Abbreviation/code	Working dilution (IF)
Anti-IBV	JH3006	1:100
Anti-IBV E	JH3012	1:500
Anti-IBV M	JH1643	1:250 or 1:500
Affinity-purified anti-M	AP35B	1:40
Anti-IBV N	1154-1 (E. Collisson)	1:100 or 1:200
Anti-IBV S	JH4926	1:500

Table 9c.

Secondary antibodies	Source	Working dilution (IF)
Goat anti-Mouse IgG coupled to Alexa 488	Jackson Labs	1:50
Goat anti-Mouse IgG coupled to Alexa 596	Jackson Labs	1:50
Goat anti-Rabbit IgG coupled to Alexa 488	Jackson Labs	1:50

3.11. Inhibitors

Brefeldin A (BFA) is a fungal compound isolated from *Penicillium brefeldianum*. By preventing the association of COPI-coats with IC and *cis*-Golgi membranes it disassembles the Golgi stacks within minutes and interferes with protein transport from the ER to the Golgi complex [79]. Notably, the IC persists after BFA treatment and maintains its association with the endocytic recycling system [80] [66].

3.12. Software

The software used here was the AxioVision Imaging System (based on release 4.5, 12/2005) configured to the Zeiss Axiovert 200M microscope equipped with 63x and 100x oil immersion objectives, i.e., the objectives used in most of the current experiments.

4. METHODS

The flow chart below summarizes the basic methods used in the experiments involving the use of the epithelial Vero cells as host cells for IBV infection to obtain information of the pathway that CoVs use for their transport from the IC to the extracellular space.

```
Uninfected Vero cells  ──────────►  Infected Vero cells
        │                                   │
        ▼                                   ▼
  Storage of cells                   Passage of host cells
        │                                   │
        ▼                                   ▼
   Cell passage                        Virus dilution
        │      ╲                            │
        ▼       ╲                           ▼
   Fixation  ◄── Drug treatment         Infection
        │ ╲                              ╱    │
        ▼  ╲                            ╱     ▼
Guanidine-HCl treatment ◄── Blocking and permeabilization    Fixation
             ╲                                                  │
              ╲                                                 ▼
               ╲                                      Staining with antibodies
                ╲                                                │
                 ▼                                               ▼
Staining with antibodies        Plaque titration            Microscopy
        │                             │                         │
        ▼                             ▼                         │
   Microscopy              Calculation of virus titer           │
        │                             │                         ▼
        ▼                             ▼
Evaluation of results      One-step growth curve      Evaluation of results
```

```
II.  ┌──────────┐
     │   IBV    │
     └──────────┘
           │
           ▼
   Stock preparation
           │
           ▼
   Storage (-80⁰C)
```

Flow chart summarizing the cells, virus and various methods used in this study

4.1 Storage of Vero cells

The cells grown in 75 cm^2 flasks were retrieved from the 37°C CO$_2$-incubator, the growth medium was removed by suction and the cells were washed with 10 ml of PBS to remove the serum containing trypsin inhibitors. 5 ml of trypsin-EDTA was added to each flask of which about 4 ml was removed by suction, leaving a small volume to keep the cells covered for effective trypsinization. The cells were viewed in the microscope to observe the effects of trypsin. After the cells rounded up, the flasks were gently hit to loosen up the cells and 10 ml of complete growth medium (see below) was pipetted into the flasks containing the loosened cells which were mixed by pipetting. The suspended cells were transferred into 15 ml tubes and pelleted by centrifugation for 3 min at 1000 rpm. The supernatant was removed by suction, the pelleted cells were carefully resuspended in the ice-cold DMEM containing 10% DMSO and 40% FCS (freezing medium) and the cell suspension was aliquoted in 1 ml portions into cryotubes. The tubes were first placed in the -20°C freezer for 3 hours, then frozen down overnight at -80°C in a controlled fashion in a Nalgene cryo-freezing container and finally transferred to a liquid nitrogen tank for long-term storage at 196°C.

4.1.1. Thawing of cells

At regular intervals, individual cell vials were retrieved from the liquid nitrogen tank and thawed in a 37^{0}C water bath. The cells were transferred into a 15 ml tube containing 10 ml ice-cold complete growth medium and pelleted by centrifugation for 3 min at 1000 rpm. Then, the supernatant containing DMSO was removed by suction. Finally, the cells were resuspended in 5 ml of fresh growth medium and placed into 25 cm^2 cell culture flask for growth.

4.2 Cell culture

4.2.1. General maintenance of Vero cells

Vero cells were grown at 37°C in 5% CO$_2$ atmosphere. The complete growth medium was DMEM supplemented with 10% FCS heat inactivated, 2 mM L-glutamine, and 50 units/ml penicillin and 50 µg/ml streptomycin. The cells were grown in a 25 cm^2 filter-capped culture flasks until they reached about 70-95% confluency depending on the experiment. The growth and maintenance of cells, as well as other experimental processes involving the cells were performed under sterile conditions. All solutions used in the project were either purchased sterile or sterilized by filtering through a 0.2 µm pore size filters before use.

4.2.2 Cell passaging

The cell cultures were monitored daily using a light microscope equipped with phase contrast optics to check for confluency. The cells were routinely passaged at 60-90% confluency. During the passaging, the cells were rinsed with PBS, and released by the addition of trypsin-EDTA as described above. Cell aggregates were disrupted by rigorous pipetting after addition of complete growth medium into the flasks. The cells were split into new 25 cm^2 flasks in a fresh growth medium at dilutions ranging from 1:2 to 1:10, depending on the confluency of the culture used for passaging. The newly split cultures were put back in the CO$_2$-incubator for growth and further passaging, or for use in experiments.

4.3 Sample preparation for immunofluorescence microscopy

In general, for the immunofluorescence staining experiments, cells were plated on glass coverslips in 6-well plates, grown for 1-2 days until they reached a confluency of about 60-80% and then fixed with PFA. The fixation of cells must be done properly because incompletely fixed samples can develop artifacts. The antibodies used for double-staining must be checked for eventual cross-reactivity.

4.3.1. Plating of cells on coverslips

The cells retrieved from the CO_2-incubator were examined under a light microscope equipped with phase contrast optics to ascertain the confluency of the cell monolayer. The cells were released by trypsinization as described above and resuspended in fresh complete growth medium at about 1:5 dilution. 2 ml of the cell suspension was added in each well of the 6-well plates containing a coverslip and the plates were placed for 2 days in the CO_2-incubator.

4.3.2. Fixation of cells with PFA

At the end of the 2-day incubation, the 6-well plates were viewed in the microscope to ensure that the cells were in good condition. The medium was removed by suction and 2 ml of the fixative (3% PFA in 0.1M phosphate buffer, pH 7.2) was pipetted in each well. To make the fixative, 3 g of PFA powder was dissolved in 50 ml MilliQ water to which 5 drops of 1 M NaOH was added, and which was slowly heated to 60° C. When the PFA had dissolved and the solution became clear, 50 ml of 0.1 M Phosphate buffer pH 7.2 was added to adjust the pH. The fixative was finally passed through two filter papers (Whatman) in a funnel. The standard fixation time was 60 min, whereafter the cells were washed once with washing buffer (PBS + 0.2%BSA).

4.3.3. Guanidine-HCl treatment, blocking and permeabilization of the cells.

The washing buffer was removed by suction and 50 µl of 6 M guanidine-HCl in 50mM Tris-buffer, pH 7.5 was pipetted onto each coverslip, resulting in the case of some antibodies in the retrieval of antigenic sites. After the 5 min guanidine-HCl treatment, the cells were washed extensively (5 times) with PBS to remove all salt. Then, 700 µl of blocking buffer – i.e., washing buffer supplemented with 0.2% saponin and 5% goat serum (filtered through a 0.2 µm Millipore filter) – was pipetted into each well to permeabilize the cells and to block unspecific binding of secondary goat antibodies, followed by incubation for 60 mins on a shaker at RT^0C.

4.3.4. Staining of the cells with antibodies

After blocking and permeabilization, the medium was removed by suction, the immediate surroundings of the coverslips were dried by suction and 40-50 µl of antibody in blocking buffer was pipetted onto each coverslip (see Tables 10a-c for the lists of primary and secondary antibodies), followed by incubation for 60-120 min or overnight – in the latter case in a humid chamber. The cells were then washed 4 times with washing buffer (PBS with 0.2% BSA, 0.2% saponin and 0.02% azide) and left on a shaker for about 2 hrs. The medium was then removed and as described above, 45 µl of secondary antibody was added on each coverslip. The plates were kept for 90 min in the dark covered with a foil. Cells were rinsed again with the washing buffer and then left in the last wash for 2 hrs on a shaker (still covered with foil).

In the experiments where double staining was carried out, the incubation with the two antibody pairs (primary antibody and the secondary fluorochrome-coupled antibody) was carried out successively, involving the steps described above. After the stainings were completed, the cells were washed twice with PBS, followed by mounting on clean objective slides in a drop of Vectashield Mounting Medium containing the DNA stain DAP1.

4.3.5. Microscopy and image acquisition

The antibody-stained cells were examined in Zeiss Axiovert 200M inverted microscope equipped with long working distance (LD) objectives, phase contrast capability, AxioCam HRm camera and fluorescence filters which were appropriate for DAPI and the two fluorophores used in this study, Alexa 488 (green channel) and Alexa 596 (red channel), coupled to the secondary anti-rabbit or anti-mouse antibodies.

Three objectives were alternatively used to view the cells. For imaging of a large number of cells at low magnification, the LD plan-NEOFLUAR 20 X/4.0 Ph2 dry objectives was used. Most experiments involved use of the two oil immersion objectives for imaging of the cells at higher magnification: LD Plan-NEOFLUAR 63X/0.75 Ph2 and Plan-NEOFLUAR 100X/1.30 Ph3.

Zeiss Axiovert 200M is an inverted microscope. Thus, the filtered light of appropriate wavelength enters the specimen from the top and excites the fluorophore. The fluorophore receiving light of a certain wavelength changes the structure of its atomic shell, leading it to emit light of another (longer) wavelength. Alexa 488 is excited by blue light and emits green light, whole Alexa 596 is excited by green light and emits red light. The excited light from the stained specimen passes down through the objective lens system to reach the eyes or the camera.

4.4 Treatment of cells with brefeldin A

After reaching about 70-90% confluency the cells on coverslips were treated for 60 min with BFA by adding 2 ml of prewarmed complete growth medium containing 5µg/ml of the drug, while other coverslips served as untreated controls. After the treatment, the cells were fixed for 60 min with PFA. Following permeabilization and blocking, the cells were double-stained for IC (Rab1) and RE (Rab11, TfR) markers as described above.

4.5 Preparation of IBV stocks

The virus used in this work was provided by Prof. Carolyn Machamer. Upon arrival, the virus was stored in the -80^0C freezer. For stock preparation, one of the virus-containing tubes was retrieved from the freezer; the virus was thawed in a 37^oC water bath and kept on ice. Vero cells grown in two 10 cm diameter culture dishes were washed once with plain DMEM to remove the serum. The virus (250µl) was mixed with plain DMEM to give a final dilution of 1:8, whereafter 1ml of the virus dilution was added into each culture dish and gently mixed to spread the virus over the whole cell monolayer. The two dishes were then placed for 60 min in a CO_2-incubator and gently mixed at every 10 min to keep the cell monolayer covered with the medium. Thereafter, the virus-containing medium was removed and 6 ml of prewarmed DMEM containing 2% FCS was added to each culture dish, which were incubated at 37^oC in a CO_2-incubator for about 20 hrs until syncytia started to form based on viewing in the

microscope. At harvest, the dishes were covered tightly with Parafilm and subjected to 3x freezing (at -80^{0}C) and thawing (warm plate at 37°C) to release intracellular progeny virus particles, as well. Thereafter, the virus-containing homogenates were mixed carefully with a micropipette, transferred into two 15ml tubes and the contents of the tubes were vortexed extensively and centrifuged for 15 mins at 2000 rpm. The supernatants were divided into 250 µl and 500 µl aliquots in sterile 1.5 ml tubes, which were stored in the -80°C freezer for future use.

4.5.1. Plaque assay for virus titration

Plaque assay is an important method in virology. It is used to quantify the number of infectious virus particles in a given sample. The number is given as plaque forming units (PFU)/ml. In the present study, plaque titration was first carried out to determine the number of infectious particles in the newly prepared virus stock. For this purpose, Vero cells in 6-well plates were grown for 2 days to reach ~ 95% confluency. The wells were labelled to indicate the dilutions from 10^{-1} to $10^{-6.}$ An aliquot of the virus stock was retrieved from the -80^{0}C freezer and thawed in a 37°C water bath. Ten-fold serial dilutions were prepared in 1.5 ml microfuge tubes (see Results, Figure 8) with careful mixing in between. The cells in the 6-well plates were rinsed with serum-free medium and 200 µl of the virus dilution was added into each well and properly mixed to cover the monolayer. The plates were placed for 60 min in the CO_2-incubator for virus infect-ion to take place and rocked at 10 min intervals. Meanwhile, the 1.8% agarose solution was melted in the microwave oven and kept at 55°C in a water bath. 2x DMEM containing 4% FCS was prewarmed and kept in a 37°C water bath until the end of adsorption. Towards the end of infection, the agarose was put for about 90 sec at RT^{0}C to cool to about 45°C, whereafter; equal volumes (20 ml) of prewarmed 2x medium and agarose were mixed. Subsequently, the virus inoculums were aspirated, and 2 ml of the agarose-medium mix was gently added into each well and allowed to solidify for about 2 min. After solidification, the plates were kept in the CO_2-incubator for 2-3 days to allow for plaque formation. After the incubation, the plates were put for 30 min in the refrigerator. Thereafter, the solid agarose overlay was removed with a spatula and the cells in each well were stained for 10 min with 1 ml of crystal violet solution (0.05% crystal violet in 20% EtOH). The staining solution was removed by suction and the wells were rinsed with ddH$_2$O and allowed to dry.

4.5.2. Determination of virus titer

The number of plaques was counted from the wells/dilutions containing an easily calculable number (10 - 50) (see Results, Figure 8). With the formula shown below, the titer (PFU/ml) of the virus stock (or a medium sample containing released virus; see below) was calculated:

$$\frac{\text{Number of plaques}}{D \times V} = \text{virus titer (PFU/ml)}$$

Where: D = dilution factor

V = ml of diluted virus added per well

Standard volume of diluted virus per well in this work was 0.2 ml.

4.5.3. Infection of Vero cells with IBV
Vero cells grown on coverslips were infected with IBV to test the effect of virus dilution on efficiency of the infection as well as the properties of the IBV antibodies (see Table 9b).

In the first case, Vero cells added at appropriate dilutions onto coverslips were grown for 2 days to reach 60-70% confluency. Aliquots of our own IBV stock were retrieved from the -80°C freezer and thawed in a 37°C water bath. Different dilutions of the stock (1:4, 1:8, 1:16) were prepared and 50 µl of the diluted virus preparations were pipetted on each coverslip, while some coverslips received undiluted virus. The plates were incubated for 60 min for the infection to take place while mixing at 10 min intervals. After the infection, the virus inoculum was removed by suction and the coverslips were washed once with prewarmed plain DMEM. After the wash, 2 ml of growth medium (DMEM + 2% FCS) was pipetted into each well and the plates were kept for 8 hr in the CO_2-incubator. At harvest, the cells were fixed for 60 min with 2 ml of 3% PFA. After the fixation, the cells were rinsed twice with washing buffer (PBS with 0.2% BSA). Following permeabilization and blocking, the cells were stained for 120 mins with anti-N antibodies (1:200). After appropriate staining with secondary antibodies, the coverslips were mounted on microscope slides in Vectashield Mounting Medium containing DAPI.

4.5.4. Testing of IBV antibodies
The testing of the IBV antibodies first involved single staining of infected Vero cells for the determination of their suitable working dilutions (see Table 9b). Furthermore, double staining with rabbit anti-M antibodies and different organelle markers (IC, RE and lysosome) was carried out. In some experiments, overnight staining with affinity purified anti-M was carried out using 1:40 dilution of the antibody. The mouse antibodies against organelle markers included: anti-ERGIC-53 (1:200), anti-Rab1 (1:200), anti-Rab11 (1:50), anti-TfR (1:200) and anti-LAMP1 (1:100). Incubation was overnight in a humid chamber at RT^{0}C.

4.5.5. Determination of the one-step growth curve of IBV
By applying plaque titration, the growth curve for IBV was generated in this work to determine the kinetics of virus release. In addition, we examined the effect of low temperature (31°C) on virus release. The infection of Vero cells with IBV was done as described above (4.5.3). The virus dilution of 1:4 was employed to reduce the concentration of FCS, which is inhibitory to virus adsorption. To obtain efficient one-step infection, the multiplicity of infection (MOI) of 1 PFU/ml was used. For the generation of the growth curve, following the 60 min infection with IBV, 1 ml of prewarmed growth medium (DMEM + 2% FCS) was added into each well and the plates were placed in the CO_2-incubator. At regular intervals (2, 4, 6, 8, 10, 12, 14 and 16 hr), medium samples were harvested. The samples were put in 1.5 ml microfuge tubes and spinned for 60 sec at 13,000 rpm in an Eppendorf table-top centrifuge. The supernatants were frozen in 100 – 500 µl aliquots at -80^{0}C. The low temperature incubation of infected cells was carried out on water bath at 31°C in medium (DMEM + 2% FCS) was supplemented with 20mm HEPES, pH 7.2 to maintain the pH. Plaque titration of the medium samples was done as described above.

4.6 Confocal imaging

The cells were monitored using the Leica TCS SP8 STED 3X confocal system equipped with a 100 x oil immersion objective (numerical aperture 1.4). For standard fixed samples such as those used here, the 100 x oil STED WHITE is the best objective lens to use because of its high-resolution power and excellent performance that goes up to 30 µm deep into the sample. For co-localization analysis of IBV M protein with Rab1 and TfR, a single STED line and fluorescent labels with different emissions were used. The lasers used were blue diode laser for DAPI excitation (405 nm), white laser for excitation of the green fluorophore (Alexa 488), and STED-laser 1 for the red fluorophore (Alexa 594). The Lightning Software module was used for adaptive deconvolution which improves confocal images by mathematical algorithms towards a resolution of 120 nm.

5. RESULTS

As discussed above, various studies and experiments have addressed the process of entry of CoVs into their host cells. By contrast, the endomembrane compartments that operate in the cellular exit of these viruses – during their transport from the IC to the extracellular space – are less well understood. For a long time, it has been commonly thought that CoVs employ the Golgi-dependent classical secretory pathway for their release from the infected cells. However, alternative routes for virus exit have also been recently suggested, involving the endocytic recycling system and/or the lysosomal compartment [81] [21]. It was therefore of interest to investigate the role of the endolysosomal membrane system in CoV release, as well as to find out if their exit occurs in a Golgi-dependent or Golgi-independent fashion. These considerations explain the choice of the endogenous organelle markers that were characterized and used in the experiments described below.

5.1 Testing of antibodies against organelle markers in Vero cells

First, several antibodies against the IC, RE and lysosomal markers were tested in the green monkey kidney (Vero) cells, which were used here as host cells for IBV. It was of particular interest to identify monoclonal antibodies that work well in Vero cells and therefore could be used in double staining as pairs for the CoV antibodies (obtained from Prof. Carolyn Machamer; see below), which have all been prepared in rabbits. The antibodies were tested in different dilutions and using various fixation and permeabilization conditions. Good results were obtained with monoclonal mouse antibodies against a set of organelle markers that are briefly introduced in the following.

5.1.1. IC/cis-Golgi Markers

p58/ERGIC-53 – a non-glycosylated single-spanning membrane protein – was the first marker protein of the IC to be identified [82]. Rat p58 and its human homologue ERGIC-53 function as cargo receptors during the exit of newly synthesized mannose-containing cargo proteins from the ER, facilitating their transport to IC/*cis*-Golgi. These proteins become enriched in the IC elements due to their continuous cycling between ER exit sites (ERES) and *cis*-Golgi [83] [80]. p58/ERGIC-53 consists of a large luminal part containing the carbohydrate recognition domain (CRD) which is crucial for the binding of glycoprotein cargo, a transmembrane domain, and short cytoplasmic tail. The latter harbors a conserved KKFF (-Lys-Lys-Phe-Phe) sequence at its C-terminus which plays an important role in the bidirectional trafficking of the protein [84].

Rab1 is a member of the large family of regulatory Rab GTPases, which play key roles in various steps of membrane trafficking. They specifically associate with different organelles of the endomembrane system and are considered to give organelles their identity. Rab1 specifically associates with the IC and regulates bidirectional transport at the ER-Golgi boundary [85]. The two isoforms of Rab1 – Rab1A and Rab1B – share about 92% identity at the amino acid level and may be rather similar in their biochemical functions and properties [86] [87]. The function of Rab1 is also crucial for the biogenesis and maintenance of the Golgi apparatus and its over-expression leads to enlargement of the Golgi [88]. Immunogold labeling of NRK cells showed the localization Rab1 to tubulovesicular IC elements and the *cis*-most cisterna of the Golgi stacks [89].

5.1.2. Markers of recycling endosomes and lysosomes

Rab11, another member of the Rab GTPase family, is the best characterized marker for recycling endosomes (REs). Initially, some studies suggested that Rab11 functions in the post-Golgi secretory pathway between the *trans*-Golgi network (TGN) and the cell surface until it was established that it is in fact a specific marker for the endocytic recycling system [90]. It is localized to peripheral REs and the pericentrosomal endocytic recycling compartment (ERC) and operates in membrane recycling back to the PM. However, its localization pattern varies in different cell types which has complicated the determination of its exact functions in intracellular membrane transport [91]. There are indications that Rab11 is needed by many transport pathways that begin at the ERC. However, the mechanisms by which it regulates endocytic recycling remain only partially under-stood [90]. Expression of the dominant negative mutant form of Rab11 (Rab11S25N) reduced the rate of transferrin recycling in Chinese hamster the ovary cells, while the internalization of the transferrin was unaffected [92].

Transferrin receptor (TfR) is a well-characterized recycling single-spanning PM protein, which binds the iron-carrier protein transferrin at the cell surface and mediates its cellular uptake via receptor-mediated endocytosis [90]. As receptor-bound transferrin enters the endocytic pathway, the acidic pH in the lumen of endosomes induces the release of the bound iron, while the iron-free carrier protein (apotransferrin) remains attached to its receptor. The receptor-apotransferrin complex then enters tubular extensions of endosomes and is recycled back to the PM [90]. The recycling of TfR can take place either from the early endosomes (short loop), or from the pericentrosomal ERC (long loop).

Lysosome-associated membrane protein-1 (LAMP-1), a glycosylated type I integral membrane protein, is an abundant component of the lysosomal membrane. Together with LAMP-2, this protein has been estimated to correspond to approximately 50% of all proteins of the lysosome membrane [93] [94]. LAMP-1 has a luminal domain which is heavily glycosylated, a trans-membrane domain and a short C-terminal cytoplasmic tail [93]. Following its synthesis, LAMP-1 is transported to the *trans*-Golgi network (TGN) for further sorting and delivery to the lysosomes. It functions in the maintenance of the structural integrity of the lysosomal membranes, maintenance of the acidity of the lysosome and protection of the lysosome from autodigestion [94].

5.2 Immunofluorescence microscopy (IF) of the organelle markers in Vero cells

Immunofluorescence microscopy was carried out to determine the applicability in Vero cells of a number of available antibodies against different markers for the intracellular compartments of interest for the present study. To identify appropriate markers for the IC/*cis*-Golgi, mouse anti-ERGIC-53, affinity purified rabbit anti-Rab1, as well as a mouse antibody against Rab1 were tested. For the endocytic recycling pathway, mouse anti-Rab11, monoclonal rabbit anti-Rab11 and mouse anti-TfR were tested. Moreover, mouse anti-LAMP-1 was tested as a possible marker for late endosomes/lysosomes. The IF staining was carried out on Vero cells grown on coverslips to reach about 70-80% confluency (for details see Materials and methods). Importantly, the three antibodies tested against markers of the IC/*cis*-Golgi membranes all worked well in these cells (Fig. 7), giving similar staining patterns as previously observed in other cell types. Whereas all highlighted the *cis*-Golgi region, the two antibodies against Rab1 also detected peripheral IC elements (Figs. 7C and D, arrowheads). A cytosolic pool of Rab1 was detectable as faint diffuse staining (Fig. 7C). It should also be noted that the *cis*-Golgi staining patterns of anti-p58/ERGIC-53 and anti-Rab1 were similar, but not identical.
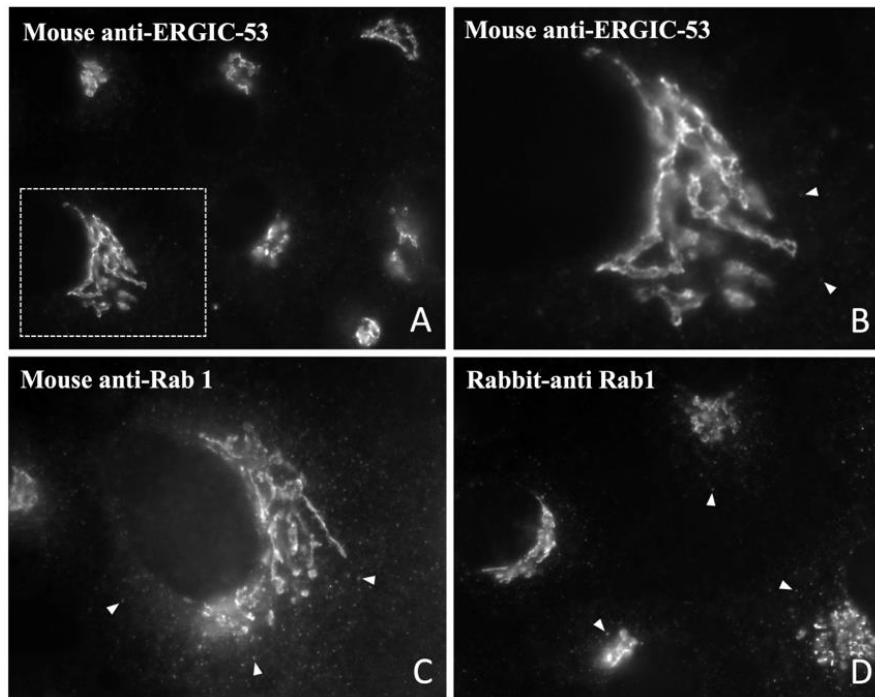
Figure 7. Immunofluorescence microscopy of IC/*cis*-Golgi markers in Vero cells. The cells grown on glass coverslips to 80% confluency were fixed, permeabilized and stained with antibodies against ERGIC-53 (A and B) or Rab1 (C and D). Both antibodies highlight the Golgi ribbon (*cis*-Golgi), whereas the mouse and rabbit antibodies against Rab1 also show the peripheral IC elements (arrowheads in C and D), which are also more weakly detected by anti-ERGIC-53 (arrow heads in B). B shows at higher magnification the Golgi ribbon indicated with a dashed area in A.

The tested antibodies against RE markers also worked well in Vero cells, with the exception of the mouse anti-Rab11 antibody, which after the routine saponin permeabilization gave only very weak fluorescence signal (Fig. 8A). Hence, pre-treatment of the fixed cells guanidine-Hcl was done (see Materials and methods), giving rise to strong staining of the ERC (Fig. 8B and C, open arrowheads), similar to that obtained with the polyclonal rabbit anti-Rab11 (Fig. 8D). In addition to the pericentrosomal ERC, the antibodies against the RE markers – including the mouse anti-TfR anti-body (Fig. 8E) – all high-lighted individual REs scattered throughout the cytoplasm (Fig. 8B-E).

Finally, the lysosomal marker LAMP-1 was included in our work due to the recent paper providing evidence that CoVs utilize the lysosomal compartment for their cellular exit [81]. Like mouse anti-Rab11, the mouse anti-LAMP-1 antibody also required the guanidine-HCl pre-treatment of fixed cells to work. Under these conditions the antibody gave punctate staining of the lysosomes concentrating in the perinuclear region (Fig. 8F).
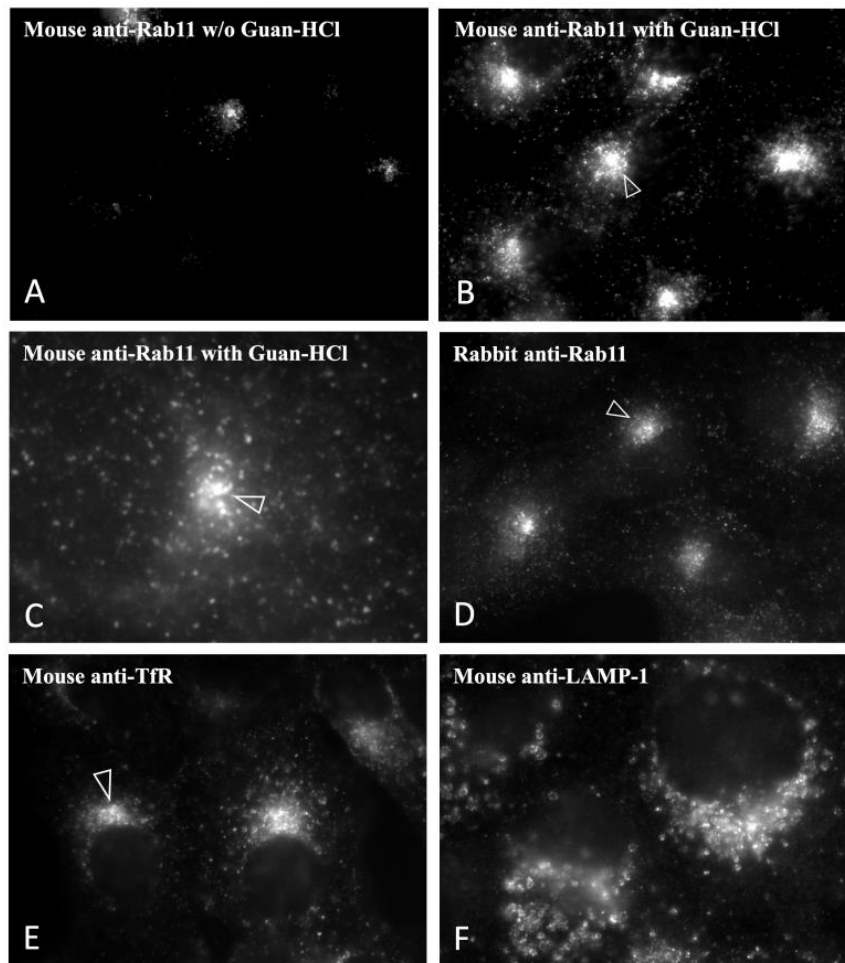
Figure 8. Immunofluorescence microscopic localization of markers for recycling endosomes and lysosomes in Vero cells. The mouse and rabbit antibodies against Rab11 (A-D) or TfR (E) all highlight the perinuclear endocytic recycling compartment (ERC; open arrowheads) next to the centrosome, as well as individual recycling endosomes scattered throughout the cytoplasm. Note that the mouse anti-Rab11 antibodies only work well, when the fixed cells are pretreated with guanidine-HCl (compare A and B). (C) shows the pericentrosomal ERC at higher magnification. (F) Labeling of perinuclear lysosomes by the mouse antibody against LAMP-1.

Based on the above results, we could conclude that all the mouse antibodies tested against relevant organelle markers could potentially be applied in the further experiments with IBV-infected Vero cells. Furthermore, having established the applicability of the markers of interest, treatment of Vero cells with brefeldin A (BFA, 5 µg/ml) was carried out, followed by double staining with antibodies against different IC and RE proteins (Rab1, Rab11, TfR). This experiment showed that after dis-assembly of the Golgi stacks by 60 min treatment with BFA, the spatial connection of the IC and RE elements is maintained, as described in other cell types [66] (data not shown).

5.3 Infection of Vero cells with infectious bronchitis virus (IBV)

5.3.1. The plaque assay

The plaque assay (also called plaque titration) is an important technique in animal virus research. It is a method used to quantity the number of infectious virus particles in a given virus preparation. Accordingly, the number of viruses is expressed as plaque forming units (PFU)/ml. An earlier procedure used in studies of bacteriophages (viruses infecting bacteria) was modified in 1952 by Renato Dulbecco for application in animal virology [95].
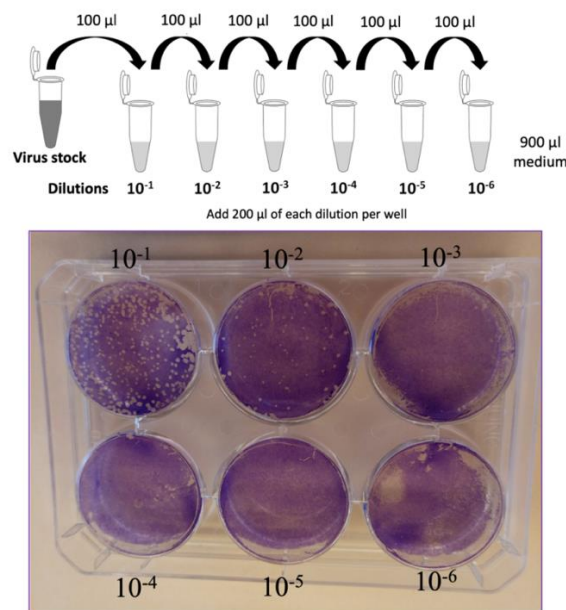

Figure 9. The method of plaque titration. First, a series of 10-fold dilutions is prepared from a virus stock (or another virus-containing sample). Subsequently, the cells in 6-well plates are infected with different virus dilutions and the cultures are overlaid with agarose-containing medium. After solidification of the agarose, the cultures are placed for 2 days in the CO_2-incubator. Due to the agarose overlay, the progeny viruses can only spread to the neigbouring cells, resulting in plaque formation. The plaques become visible after staining of the cells with crystal violet. The virus titer is determined from wells containing easily calculatable number of plaques (see Materials and methods).

The principle of this technique is described in Figure 9. After pipetting a series of 10-fold dilutions from a virus-containing sample, confluent cultures of cells in 6-well plates (as in our case) are infected with the different virus dilutions, whereafter the cultures are covered with agarose-containing medium. Following solidification of the agarose, the cultures are placed in a CO_2-incubator for two to three days. During this period, the agarose overlay enables the progeny viruses to spread to only neighboring cells giving rise to the formation of plaques, which become visible after crystal violet staining (see Fig. 8) and can thereafter be counted.

5.3.2. Preparation of one-step growth curve of IBV

We obtained the original IBV stock from Prof. Carolyn Machamer at Johns Hopkins School of Medicine (Baltimore, MD, USA). As described in detail in Materials and methods, we prepared two own laboratory stocks of IBV from this original stock and used the plaque assay to determine their virus titers. The one with a better titer was used to generate the growth curve shown in Figure 10.
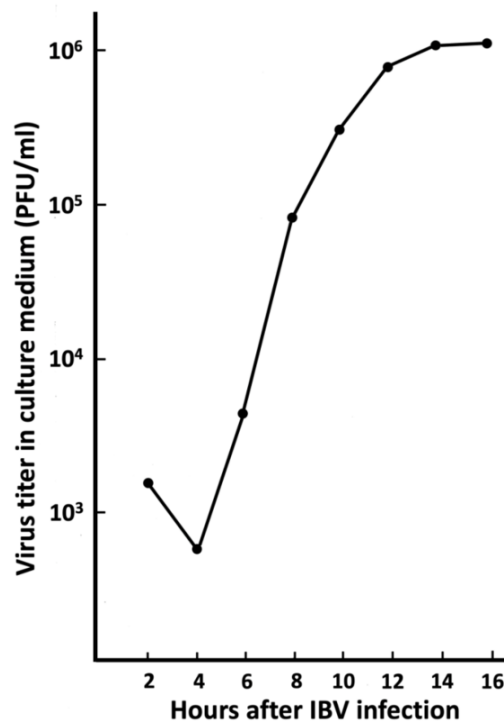

Figure 10. Determination of the IBV growth curve by plaque titration. Vero cells were infected with IBV and samples of the culture medium were harvested at the indicated time points after infection, whereafter the number of released infectious virus particles (PFU/ml) was quantified by plaque titration (see Figure 8). The curve shows the three growth phases of the virus: i) a lag phase (2 to 4hr p.i.) which corresponds to virus entry and early replication, ii) an exponential phase of virus release (4 to12hr p.i.) and the plateau phase (12 to 16hr p.i.) when virus release gradually levels off.

A one-step growth curve of IBV was determined using the new high titer virus. After infecting the cells with high multiplicity, medium samples were collected after different time periods and the amounts of released virus were quantified by plaque titration. The obtained S-shaped growth curve (Fig. 10) highlights three different phases of virus replication. First, a lag phase from 2 to 4hr p.i. when the virus penetrates the host cells and virus replication starts. The infectious virus measured in the medium during this phase does not correspond to new progeny virus, but residual extracellular viruses that remain associated with the cell monolayers after the infective virus

sample has been removed. However, after 4 hr p.i. the first progeny virus particles start to exit the cells. They are released in an exponential fashion between 6 and 12hr p.i., whereafter virus release gradually slows down and a plateau phase is reached between 14 and 16 hr. Based on the growth curve, maximum virus release occurs between 6 and 12 hr p.i. (Fig. 10).

5.4 Testing of antibodies against structural proteins of IBV

Next, the reactivities and specificities of the different rabbit antibodies against structural components of IBV (kindly provided by Prof. Carolyn Machamer, Johns Hopkins School of Medicine; see Table 9b) were examined in infected Vero cells. For this test, the cells were harvested at 8hr p.i. since based on the virus growth curve (Fig. 10) it was expected that at this time point – in the middle of the active virus release phase – the virus structural proteins would have been synthesized in sufficiently large amounts. Also, at this relatively early phase of virus replication, the cells would not yet have undergone major virus-induced alterations.

The antibodies – all whole rabbit sera – were first tested at different dilutions and appropriate dilutions (in the range 1:100 to 1:500) giving a strong fluorescence signal but minimal background was selected for further work. The IBV N-protein was readily detected by anti-IBV and anti-N antibodies (see Fig. 11A and B, respectively). Both antibodies gave diffuse cytoplasmic staining, as expected for the viral nucleocapsid. In cells at an earlier phase of infection, expressing lesser amounts of the N-protein, a punctate pattern was observed (Fig. 11A), possibly due to the association of the protein with membranous structures operating in viral RNA replication [96]. Antibodies against the viral membrane proteins E, S and M gave similar results in that they all high-lighted the Golgi area (Fig. 11C-E, asterisks). They also gave variable punctate staining throughout the cytoplasm, which at least partially corresponds to the peripheral IC elements. This pattern was most pronounced with anti-M (Fig. 11E). Antibodies against the S protein also showed some labeling of the nuclear membrane and the reticular ER (Fig. 11D).
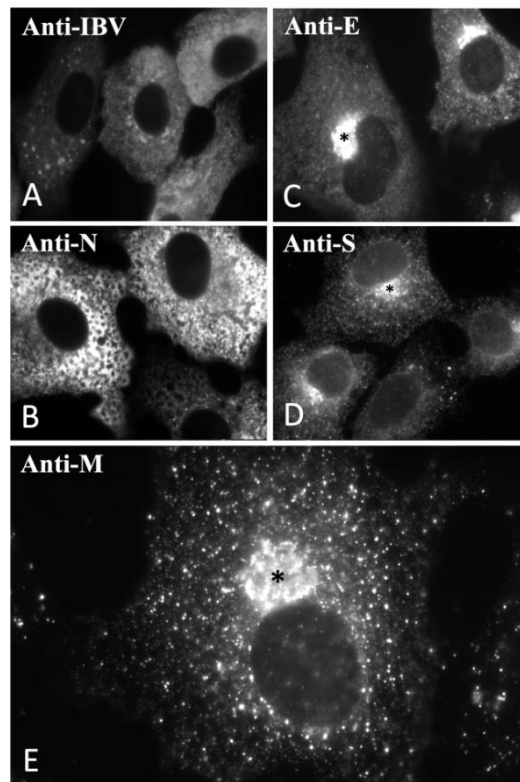
Figure 11. Testing of antibodies against IBV structural proteins in Vero cells. The cells were fixed at 8hr p.i. and stained with different polyclonal rabbit antibodies. The anti-IBV (A) and anti-N (B) antibodies both detect the IBV N-protein, showing its diffuse cytoplasmic distribution. The antibodies against viral membrane proteins: E (C), S (D) and M (E) all give staining of the Golgi area (asterisks). Anti-S also labels the ER, including the nuclear envelope, whereas anti-M highlights numerous punctate structures throughout the cytoplasm, many of which are expected to correspond to the peri-pheral IC elements.

5.5 Improving the efficiency of IBV infection

When infecting Vero cells grown on glass coverslips, we noticed that the efficiency of the infection was quite low (about 20%) and also variable from one experiment to the next. Therefore, we introduced two additional steps in the protocol to increase the efficiency of virus infection.

First, instead of adding virus in a large volume (ca. 750 µl/well) in the bottom of the 6-well plates, it was applied in a small volume (50 µl) just on top of the coverslips. This "drop method" would allow the use of the virus in a more concentrated form without depletion of our virus stocks. In this way, using the available IBV stocks, a multiplicity of infection of approximately 1 PFU/cell could be achieved. Second, we tested how virus adsorption at low temperature – keeping the 6-well plates for 60 min on ice prior to their placement in the CO_2-incubator – would affect the efficiency of infection. In this case, the virus particles were expected to gain more time to

effectively settle onto and bind to their host cells, prior to virus entry. As shown in Fig. 12, the employment of the "drop method" alone already appeared to give a partial increase in the efficiency of infection (27%), while the "low temperature adsorption method" gave an additional almost 2-fold increase (52 %). Due to these improvements, these steps were introduced in all subsequent infections.
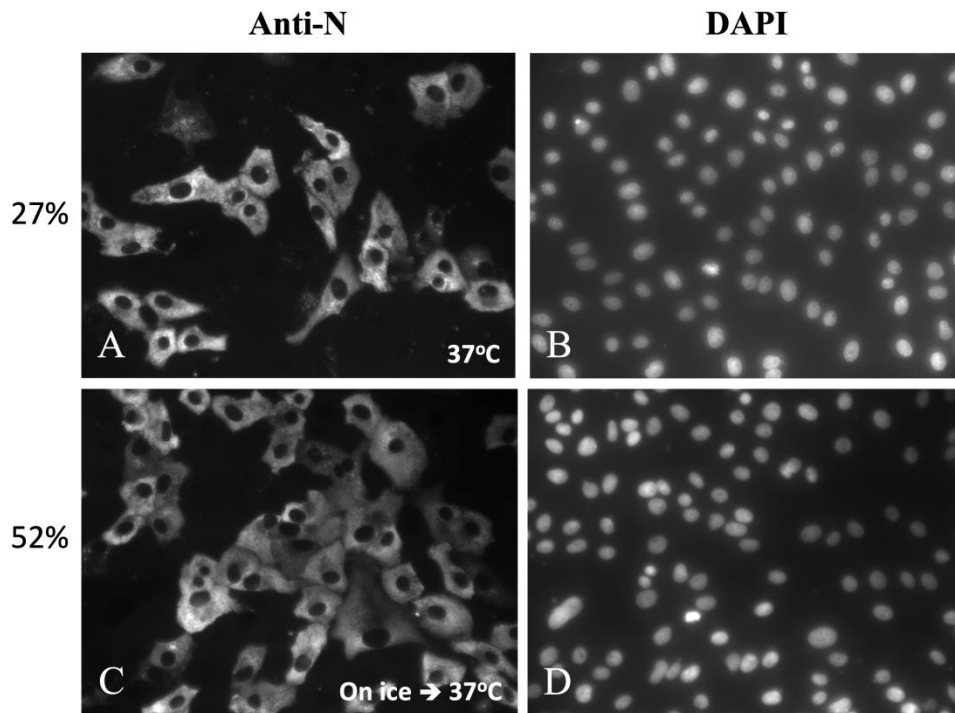

Figure 12. Improving the efficiency of IBV infection. Following the addition of virus in a small volume ("drop method") onto Vero cells grown on coverslips, the cells were either directly placed for 60 min in the 37°C CO_2 incubator (A and B), or the virus was first allowed to adsorb to the cells during a 60 min incubation on ice (C and D). The cells were fixed at 7 hr p.i. and stained with anti-N antibodies (to identify the infected cells) and DAPI (to visualize the nuclei). The infection efficiencies shown on the left reveal an about 2-fold enhancement due to the low temperature pre-treatment.

5.6 Effect of virus infection on organelle markers

5.6.1. Localization of p58/ERGIC-53 shows Golgi fragmentation

Having determined the localization of different organelle markers in uninfected Vero cells (see above; Figs. 7 and 8), it was necessary to see whether the infection of cells with IBV affects their distribution or the morphology of the different compartments where they reside. Hence, Vero cells were infected employing the drop and low temperature adsorption methods (Fig. 12), fixed at 6, 8, 10 and 12hr p.i. and double stained with anti-IBV N and mouse anti-ERGIC-53 antibodies and analyzed by immunofluorescence microscopy.
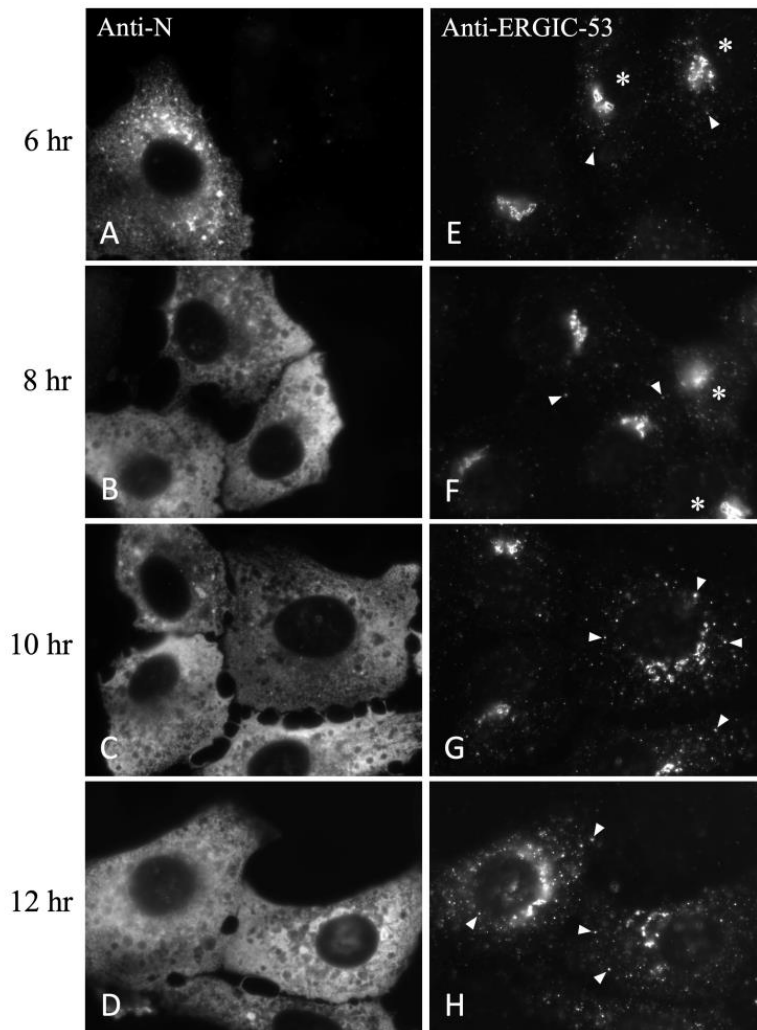
Figure 13. Immunofluorescence microscopy of IBV-infected Vero cells double stained with rabbit anti-N and mouse anti-ERGIC-53 antibodies reveals Golgi fragmentation. The cells grown on coverslips were infected employing the drop method and initial virus adsorption on ice (see Fig. 11). The cells were fixed at different times (6, 8, 10 and 12hr) p.i. for double staining with the two antibodies. N protein expression was used to identify virus-infected cells, while the uninfected cells are indicated with asterisks. Compact *cis*-Golgi staining similar to that seen in uninfected cells (see also Fig. 6) was observed at the early times of infection (E and F). The punctate staining (arrowheads) corresponds to peripheral IC elements. Note that at later times of infection (G and H) the Golgi undergoes fragmentation and the peripheral puncta (arrowheads) become stronger. Staining with anti-N antibodies (A-D) indicates that the number of cells strongly expressing this viral protein, displaying diffuse cytoplasmic fluorescence, gradually increases.

At 6 and 8hr p.i. a typical compact Golgi ribbon pattern, similar to that seen in uninfected cells, was observed (Fig.13E and F), However, at later times of infection – that is at 10 and 12hr p.i. – the Golgi apparatus became clearly fragmented (Fig. 13G and H). In addition, the staining of the peripheral IC elements significantly increased (Fig. 13G and H, arrowheads). This may indicate that the apparent dispersal of the Golgi apparatus was partly due to the redistribution of p58/ERGIC-53 from the *cis*-Golgi, where it is normally concentrated, to the peripheral IC where

virus budding takes place. Preliminary analysis of cells at the different time points gave the following percentages of cells with Golgi fragmentation: 6hr (30%), 8hr (36%), 10hr (59%) and 12hr (71%).

At the earlier time points – particularly at 6hr p.i. – the expression level of the N-protein in most of the infected cells was still low, revealing a punctate fluorescence pattern. As the infection progressed, more N-protein was synthesized, resulting in an intensive, diffuse cytoplasmic staining of the cells with antibodies against the N protein.

5.6.2. Localization of Rab1 in the infected cells

Next, double staining of infected cells fixed at 6, 9 and 12hr p.i with antibodies against IBV N protein and Rab1 was carried out to examine the effect of virus infection on Rab1 localization. Mock-infected cells were used both as a negative control for antibody staining, as well as to rule out any possible effects of the infection protocols (e.g., the low temperature incubation step) on cell or organelle morphology.

As shown in Fig. 14, the distribution of Rab1 in the mock-infected cells appeared very similar to that previously seen in uninfected cells (Fig. 7), verifying that the distribution and staining patterns of the protein are not affected by the protocols as such. At 6 hr p.i. no major differences between the infected and uninfected cells were observed, except that the fluorescence staining intensity for Rab1 appeared to increase. Subsequently, at 9 hr p.i. some of the cells showed more dispersed staining in the Golgi area, while in others the Rab1-positive Golgi elements still displayed a compact pattern (Fig. 14G). At 12 hr p.i. the fluorescence intensity for Rab1 appeared to further increase, raising the possibility that its expression is enhanced or, alternatively, its membrane-association is increased. Also, the peripheral IC elements, which showed relatively modest staining at the early times of infection (6 hr), became much brighter as the infection progressed, suggesting increased association of the protein to these membranes, where active virus budding takes place.
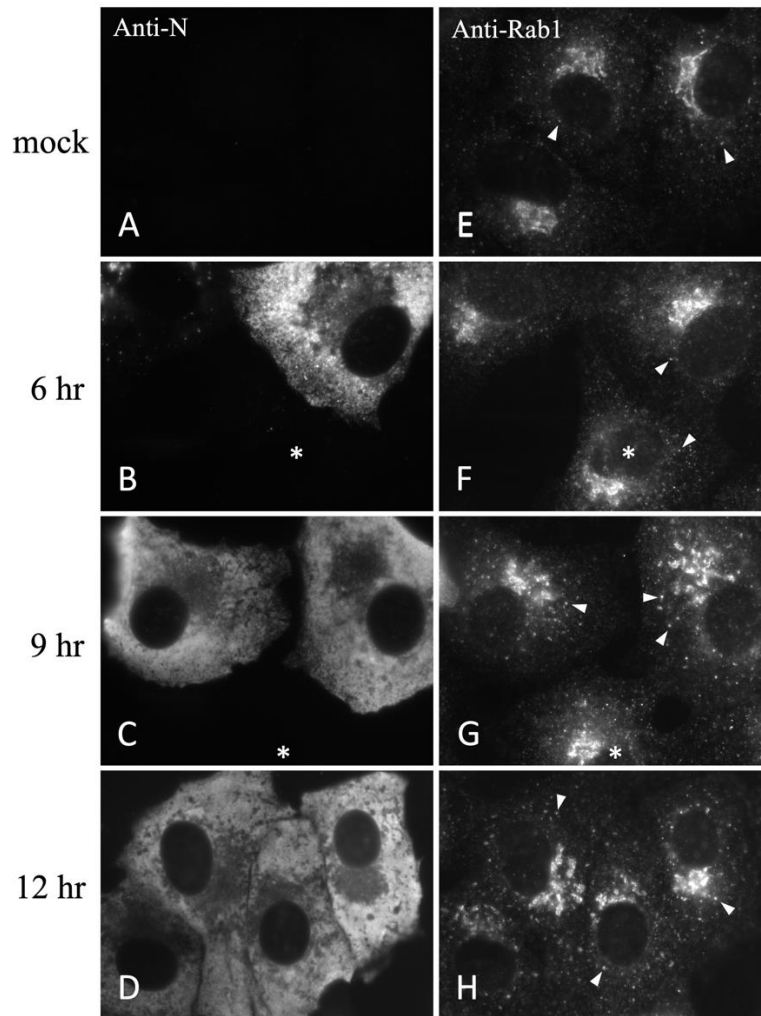
Figure 14. Localization of Rab1 during IBV infection. Vero cells grown on coverslips were infected as described for Fig. 11, employing virus adsorption on ice, and fixed at 6, 9 or 12hr p.i. for double staining with anti-N and anti-Rab1 antibodies. Expression of the N protein marks the virus-infected cells, while uninfected cells are indicated by asterisks (B, C, F and G). Whereas the Rab1 staining patterns in mock-infected cells (E) and after 6hr of infection (F) show no clear differences as compared to control Vero cells (see Fig. 6), at later times of infection, i.e., at 6hr (G) and 12hr (H) p.i., the peripheral IC elements (arrowheads) display stronger fluorescence and the Rab1-positive structures in the central Golgi area appear fragmented in some of the cells. Notably, the overall Rab1 signal in the infected cells (F-H) seems appears increased as compared to the mock-infected cells (E).

5.6.3. Localization of TfR in IBV-infected cells

Similarly, immunofluorescence double staining with anti-IBV N and anti-TfR was carried out to test for the effects of virus infection on TfR distribution using mock-infected cells and IBV-infected cells fixed at 6, 9 or 12hr p.i. As in the case of p58/ERGIC-53 and Rab1, the mock infection did not affect the fluorescence pattern of TfR (compare Fig. 15E with Fig. 8E). At the early times of infection (6hr p.i.) the pericentrosomal ERC (Fig. 15, arrowheads) showed a more diffuse pattern in some of the infected cells and a quite compact pattern in others, similar to the mock-infected and uninfected cells. Interestingly, however, as the infection progressed (9 and

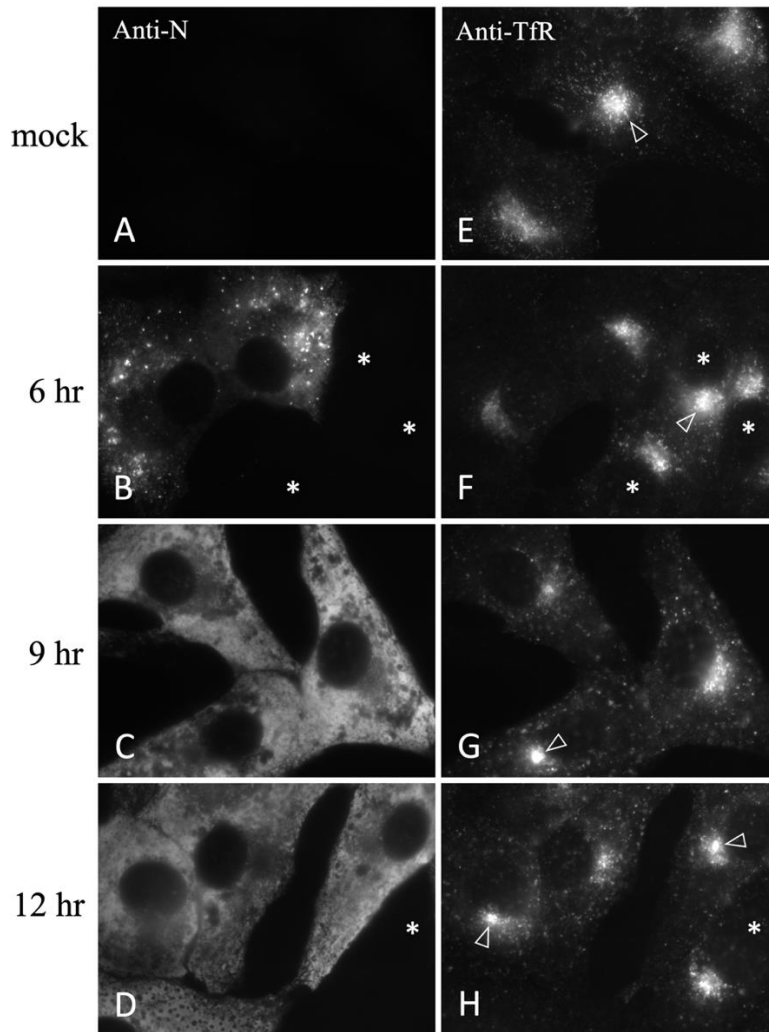12hr p.i.) the ERC gradually assumed a more compact pattern in most of the infected cells (Fig. 15G and H).

Figure 15. The effect of IBV infection on the localization of TfR. The cells infected with IBV were fixed at different times (6, 9 and 12hr) p.i. for double staining with anti-N and anti-TfR antibodies. The uninfected cells showing the absence of N protein signal are indicated with asterisks (see panels B, D, F and H). The open arrowheads indicate the TfR-positive pericentrosomal ERC, which becomes more compact in the majority of the cells as the infection progresses.

5.6.4. Compaction of the Rab11 pattern during IBV infection

Double staining of cells with anti-N and anti-Rab11 antibodies gave results that were very similar to those obtained with TfR (Fig. 16, compare with Fig. 15). Namely, as the infection progressed, the staining of the pericentrosomal ERC (Fig. 16, arrowheads) became more intensive and compact, indicating that the expression of Rab11 or its membrane-association may be affected. However, this has to be substantiated by further analysis. In parallel, staining of peripheral REs was diminished. Mock infection did not affect the distribution of Rab11, either (compare Figs. 16E and Fig. 8).
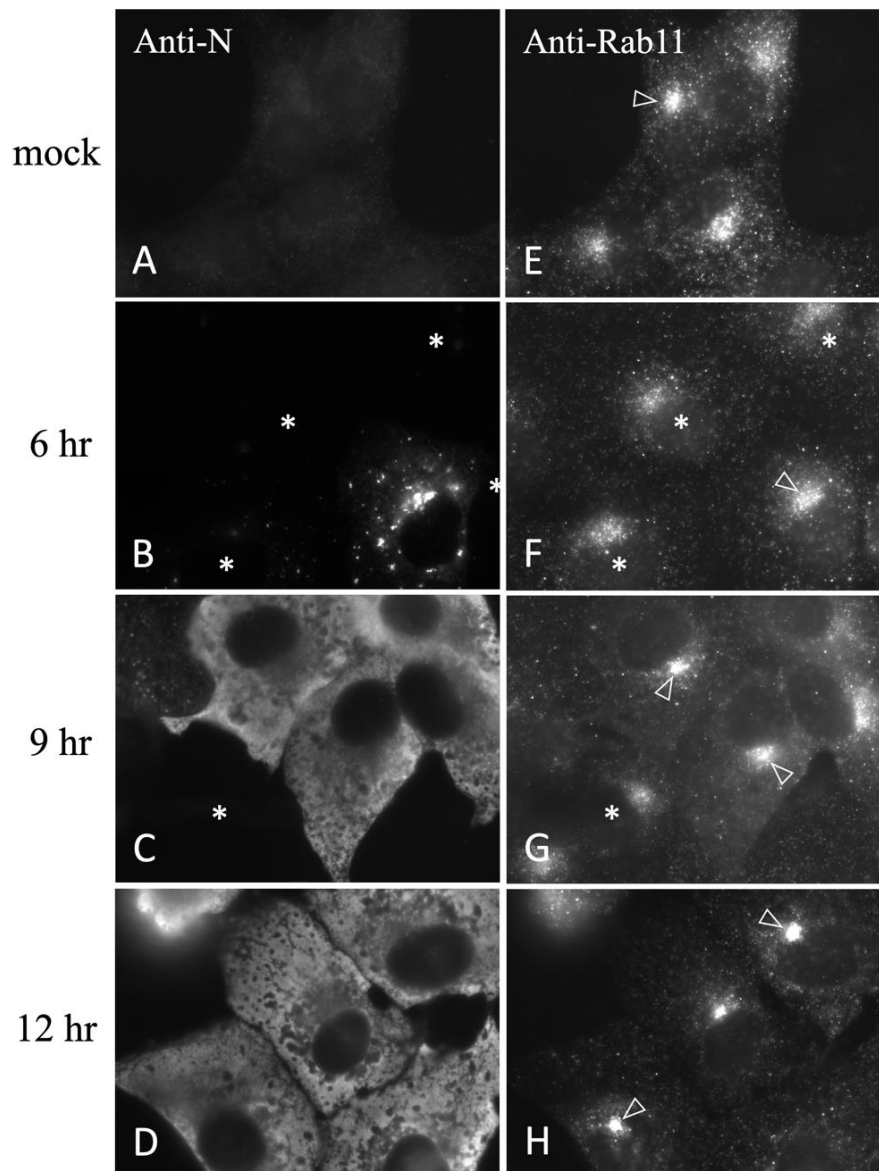
Figure 16. The localization of Rab11 changes during IBV infection. The virus-infected cells were fixed at different times (6, 9 and 12hr p.i.) for double staining with antibodies against the viral N protein and Rab11. Uninfected cells lacking N protein expression are indicated with asterisks (B, C, F and G). Very similar staining patterns, including labeling of the pericentrosomal ERC (open arrow-heads), are seen in mock- and IBV-infected cells at 6hr p.i. (compare E and F), whereas after longer times of infection the ERC signal for Rab11 gradually becomes more compact in the majority of the cells (G and H).

5.6.5. Localization of LAMP-1 in IBV-infected cells

Finally, double staining with anti-N and anti-LAMP-1 was employed to test for the effect of virus infection on LAMP-1 localization. However, in this case the results for the 9hr time point are not shown. As shown in Fig. 17, mock infection as such did not affect the distribution of the LAMP-1. At 6hr p.i. variable perinuclear localization of lysosomes was observed, as previously seen in uninfected Vero cells (Fig. 8F). Notably, at 12hr p.i. the LAMP-1 signal of the infected cells was clearly diminished. Thus, in contrast to the other markers examined, the infection has a negative

effect on LAMP-1 expression. One possibility is that the protein has been largely destroyed by lysosomal degradation. Alternatively, major redistribution of the protein – for example to the PM – could lead to apparent diminishing of its intracellular signal.
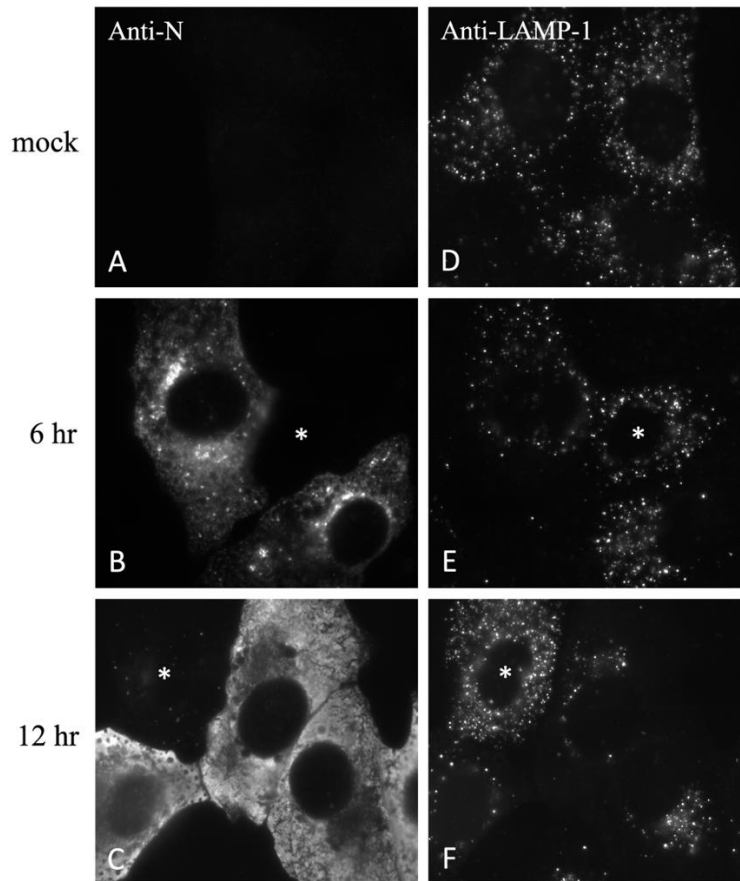

Figure 17 . IBV infection reduces the intracellular signal of LAMP-1. Following IBV infection the cells grown on coverslips were fixed at 6 and 12hr. p.i. for double staining with anti-N and anti-LAMP-1 anti-bodies. N protein expression identifies the virus-infected cells, while uninfected cells showing no N protein signal are shown by asterisks (B, C, E and F). Interestingly, while at 6hr. p.i. the LAMP-1 pattern is com-parable to that seen in the mock- or uninfected cells, by 12hr p.i. the LAMP-1 signal of the IBV-infected cells is considerably diminished.

5.7 Comparing the localization of the IBV M-protein with selected organelle markers

It was next of interest to compare the localization of the IBV M protein with some of the organelle markers described above. Rab1 and TfR were selected as markers for the IC and REs, respectively. To obtain better resolution, confocal microscopy was used for the analysis of the IBV-infected cells harvested at 9.5 hr p.i. and double stained for the M protein and the two organelle marker proteins. Knowing that after labeling of the virus-infected cells with antibodies against the M protein, approximately 90% of the signal is in virus particles [81], confocal microscopy can be expected to be a key method also in future experiments addressing the pathway of IBV release.

As shown in Fig. 18, the M protein and Rab1 showed considerable co-distribution in the perinuclear Golgi region of the infected cells. Complete overlap of the two proteins in central and peripheral structures was also frequently encountered, as indicated by the yellow colour in this merged image (Fig. 18A, arrowheads). This result was not unexpected, since the IBV M-protein is efficiently retained in the IC [43] where it mostly associates with progeny virus particles. It should also be pointed out that the Rab1- and M protein-containing central IC/*cis*-Golgi elements already appear highly fragmented at this relatively late stage of infection (Fig.13).
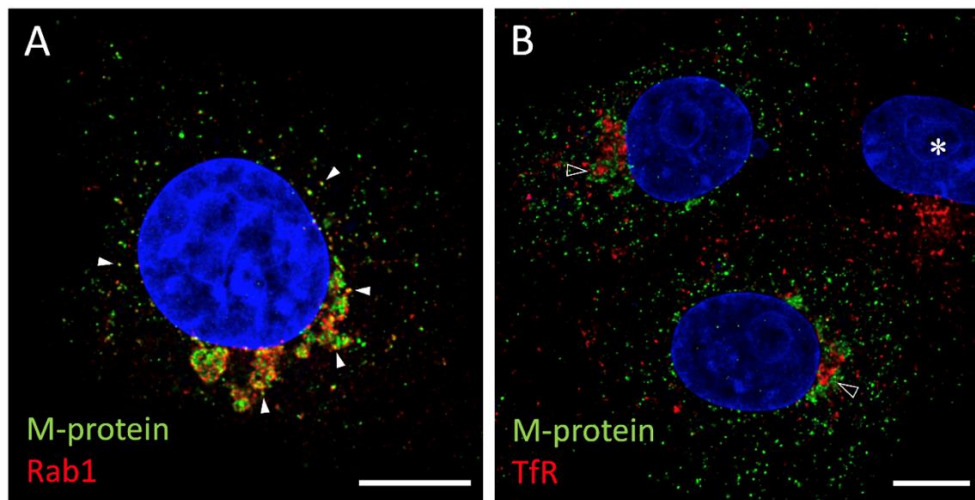

Figure 18. Confocal microscopic double-localization of the IBV M-protein with Rab1 and TfR. Cells infected with IBV were fixed at 9.5 hr p.i and double stained for the M-protein and Rab1 (A) or TfR (B). The white arrowheads in panel A denote complete overlaps of the M-protein and Rab1), giving rise to a yellow colour. Panel B shows that although there is no precise overlap between the M protein-containing IC elements and TfR-containing REs, the two types of structures display co-clustering in the juxtanuclear region (open arrowheads). The asterisk indicates an uninfected cell which only contains the perinuclear TfR signal. Scale bar: 10 µm

As the localizations the M-protein and TfR were compared, it was clear that they did not show the same kind of overlap as seen in the case Rab1. However, an apparent clustering of the M protein-containing IC elements around the juxtanuclear REs/ERC was observed (Fig. 18B, open arrowheads). As shown earlier (Fig. 16), the perinuclear ERC displayed a more compact pattern in many of the infected cells, as compared to uninfected cells (Fig. 18B, asterisk).

5.8 Effect of low temperature on IBV release

Previous work carried out by Sharon Tooze and coworkers showed that the shift of MHV-infected cells at 6-8 hr p.i. to low temperature (31ºC) does not significantly affect the budding of the virus, but efficiently inhibits release of the virus to the extracellular space [96]. The authors further

showed that the return of cells back to 37ºC lead to rapid virus release, showing that the low temperature effect is readily reversible. Since MHV is a β-CoV, it was of interest to see if the low temperature effect also applies to IBV, a γ-CoV.
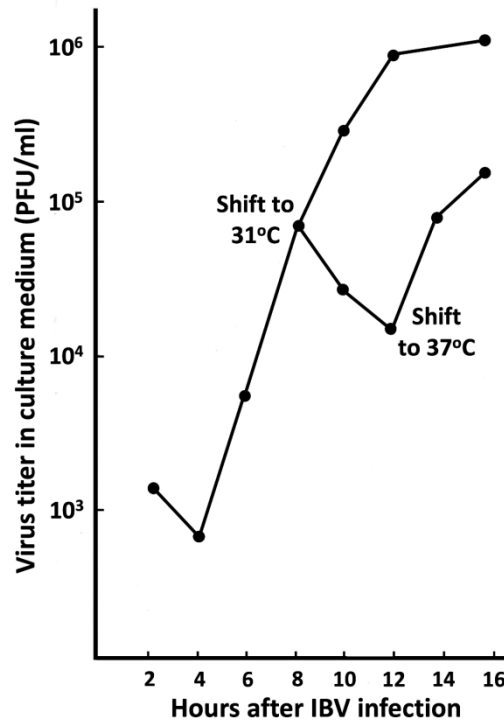

Figure 19. Effect of low temperature on IBV release. Medium samples were harvested at different times after IBV infection at 37ºC and the amounts of released viruses (PFU/ml) were quantified by plaque titration. At 8 hr p.i. some cultures were shifted to 31^0C leading to the efficient inhibition of virus release. After 4 hr at 31^0C, some of the cultures were returned back to 37ºC, revealing the rever-sibility of the low temperature effect.

Hence, we again infected Vero cells with IBV at high MOI and measured virus release by plaque titration (see Fig. 9). At 8 hr p.i. – in the middle of the exponential phase of virus release – some of the cultures were shifted for 4 hr to 31ºC, whereafter some cultures were again shifted back to physiological temperature (37ºC). Interestingly, very similar results to those reported for MHV were also obtained in the case of IBV. The experiment was repeated, but this time carrying out the first temperature shift at 6 hr, verifying the results shown in Fig. 19 (data not shown).

6. DISCUSSION

For a long time, the prevailing idea has been that CoVs are released from cells via the classical secretory pathway via the Golgi apparatus. However, recent studies have opened the possibility,

that these viruses could in fact employ another pathway for their exit – an unconventional route that bypasses the Golgi stacks. Namely, there are now more results showing that many proteins can be secreted or reach the cell surface in a Golgi-independent manner. Studies carried out by this group, as well as others, have provided evidence that such Golgi-independent trafficking is based on a direct connection between the pre-Golgi IC and the endocytic recycling pathway, bypassing the Golgi stacks completely [97]. One can distinguish between classical and Golgi-independent secretion by using BFA, a drug which rapidly breaks down the Golgi stacks. Interestingly, many unconventionally secreted proteins are delivered to the PM in the presence of this drug. Strikingly, a recent paper published in Cell showed that the β-CoV MHV is released from infected HeLa cells in a BFA-resistant manner, suggesting that this virus employs an unconventional Golgi-independent pathway for its exit [81]. Since CoVs assemble by budding into the IC lumen, it is likely that they follow the BFA-resistant direct route from the IC to the endosomal system [66] [21].

The selection of the organelle markers for this study using Vero cells was based on the above reasoning, addressing the possibility that IBV also employs direct IC-RE communication for its release. Several mostly commercial antibodies were tested and the overall results were very promising, although in some cases variations in the staining protocols had to be introduced. We were able to identify different markers for each of the membrane systems, the IC and REs/ERC. Having different characteristics they can help to investigate the events of interest from different angles, thereby providing more information. For example, the two markers p58/ERGIC-53 and TfR are both integral membrane receptors that continuously cycle in the early secretory pathway and the endosomal system, respectively. By contrast, Rab1 and Rab11 – associating with the cytoplasmic side of the IC and RE membranes, respectively – are more compartment-specific, cycling between the cytosol (inactive form) and the organelle membranes (active form).

Having established the antibodies that work well in the Vero cells, it was important to find out what happens to the distribution of the corresponding markers and compartments in the course of IBV infection. As reported earlier [98], we could show that the Golgi gets fragmented during the infection. However, the effects of IBV replication on the distribution of p58/ERGIC-53 and Rab1 were distinct. While p58/ERGIC-53 demonstrates better the fragmentation of the *cis*-Golgi over time, Rab1 shows more persistent piling up of in the juxtanuclear region. This difference could be due to the different characteristics of the markers, or the possibility that they associate with different domains of the IC/*cis*-Golgi membranes. Since the infection of cells with IBV changes the luminal conditions of the secretory compartments [99], the transport machineries that are

responsible for the cycling of p58/ERGIC-53 could be affected, resulting in its redistribution from *cis*-Golgi to the peripheral IC elements.

An important novel finding of this study, which most likely relates to the process of virus release, was the observation regarding the gradual accumulation REs – and in particular the RE-associated GTPase Rab11 – around the centrosomes in the course of IBV infection. The compaction of the ERC was already evident at 7-8 hr after IBV infection, but became more prominent between 9-12 hr, that is, towards the end of the period of active virus release. Importantly, this phenomenon was specific for the virus-infected cells and was not observed in the neighboring non-infected cells. It should be pointed out that the pericentrosomal ERC and Rab11 have been previously implicated in the assembly and/or release of various RNA viruses, such as orthomyxo- (influenza), paramyxo- (Newcastle disease virus), retro- (HIV) and bunyaviruses (Hantavirus) [100] [101], strongly suggesting that they may also participate in the late steps of CoV life cycle. It will be of interest to quantify and compare the kinetics of Golgi fragmentation and ERC compaction in the course of IBV infection to be able to determine whether they represent distinct or possibly related events.

The time frame of this study, and the prevailing circumstances, did not allow extensive application of confocal microscopy in this project. However, an encouraging pilot experiment was carried out where the localization of the IBV M protein was compared with those of Rab1 (IC) and TfR (REs). As expected, Rab1 and M protein showed extensive co-localization both in the peripheral and central IC/*cis*-Golgi elements. Notably, an apparent co-distribution of the M protein-containing IC elements and TfR-positive REs was also observed. Since approximately 90% of the M-protein signal is in intracellular virus particles [81] [102], future application of these antibodies in confocal microscopy will provide an important method to follow the transport process of virus release. Whereas the IBV M protein is efficiently retained in the IC/cis-Golgi membranes and incorporated into virus particles, the two other CoV membrane proteins have more widespread intracellular distributions [21]. Moreover, the IBV E protein has a large intracellular pool, but is present only in small amounts in the virus particles [31]

7. CONCLUSIONS AND FUTURE PERSPECTIVES

In conclusion, this study has laid down methodological groundwork for future experiments where the intracellular transport route of CoVs can be further investigated. These experiments have also

paved the way for new ideas on how the release of the CoVs from cells can possibly either be stimulated or synchronized. Since BFA does not inhibit virus release, it will for instance be of interest to compare the localizations of the M protein and the various organelle markers at different times after drug addition. Moreover, the verification that low temperature also blocks the exit of IBV opens the possibility that this approach can be used in future experiments to synchronize this process so that it can be also followed in the absence of drugs.

Since the pathway of CoV exit currently still remains poorly understood, future work based on the present results will hopefully provide novel insight on the mechanisms of virus release and in the long run contribute to the development of new anti-viral therapies.

8. REFERENCES

[1]   Harper D.R, Viruses: biology, applications and control, second edition. Garland Science, Taylor & Francis Group, 1998.

[2]   Lodish H., Berk A., Zipursky L., Matsudaira P., Baltimore D., and Darnell J. "Viruses: structure, function, and uses," in Molecular Cell Biology. 4th edition., New York, Section 6.3, 2000.

[3]   Alberts B., Johnson A., Lewis J., Raff M., Roberts K., and Walter P. Molecular biology of the cell. 6th edition. New York: Garland science, 2015

[4]   Villanueva RA, Rouillé Y, Dubuisson J. Interactions between virus proteins and host cell membranes during the viral life cycle. Int Rev Cytol. 245: 171-244, 2005.

[5]   Wisskirchen K, Lucifora J, Michler T, Protzer U. New pharmacological strategies to fight enveloped viruses. Trends Pharmacol Sci.35: 470-8. 2014.

[6]   Navaratnarajah, C. K., Warrier, R., and Kuhn, R. J. Assembly of viruses: enveloped particles. Encyclopedia of Virology. pp. 193–200, 2008.

[7]   Chen BJ, Lamb RA. Mechanisms for enveloped virus budding: can some viruses do without an ESCRT? Virology 372: 221-32, 2008.

[8]   Saraste J. "Getting to know an old enemy: the lifecycle of coronavirus," N:B:S Nytt, Bergen, pp. 5–9, 2020.

[9]   Cosset FL, Lavillette D. Cell entry of enveloped viruses. Adv Genet. 73:121-83. 2011

[10]   Muñoz-Barroso I, Durell S, Sakaguchi K, Appella E, Blumenthal R. Dilation of the human immunodeficiency virus-1 envelope glycoprotein fusion pore revealed by the inhibitory action of a synthetic peptide from gp41. J Cell Biol. 140: 315-23, 1998

[11]   Hamilton BS, Whittaker GR, Daniel S. Influenza virus-mediated membrane fusion: determinants of hemagglutinin fusogenic activity and experimental approaches for assessing virus fusion. Viruses. 4: 1144-1168, 2012.

[12]   Lenard J. Viral Membranes. Encyclopedia of virology. 308-314. 2008.

[13]   Cadd TL, Skoging U, Liljeström P. Budding of enveloped viruses from the plasma membrane. Bioessays. 19: 993-1000, 1997.

[14]   Nayak DP, Balogun RA, Yamada H, Zhou ZH, Barman S. Influenza virus morphogenesis and budding. Virus Res. 143: 147-61, 2009.

[15]   Palese P, Tobita K, Ueda M, Compans RW. Characterization of temperature sensitive influenza virus mutants defective in neuraminidase. Virology. 61: 397-410, 1974.

[16] Bavari S, Bosio CM, et. al., Lipid raft microdomains: a gateway for compart-mentalized trafficking of Ebola and Marburg viruses. J Exp Med. 195: 593-602, 2002.

[17] Scheiffele P, Roth MG, Simons K. Interaction of influenza virus haemagglutinin with sphingolipid-cholesterol membrane domains via its transmembrane domain. EMBO J. 16: 5501-8, 1997.

[18] Dubois-Dalcq M., Kathryn. V. Holmes, and Rentier B., Assembly of enveloped RNA viruses, 1st edition. Springer-Verlag Wien, 1984.

[19] Griffiths G, Rottier P. Cell biology of viruses that assemble along the biosynthetic pathway. Semin Cell Biol. 3: 367-81. 1992.

[20] Chen SY, Matsuoka Y, Compans RW. Golgi complex localization of the Punta Toro virus G2 protein requires its association with the G1 protein. Virology. 183: 351-65. 1991.

[21] Saraste J, Prydz K. Assembly, and cellular exit of coronaviruses: Hijacking an unconventional secretory pathway from the pre-Golgi Intermediate compartment via the Golgi ribbon to the extracellular space. Cells. 10: 503. 2021.

[22] Garoff H, Hewson R, Opstelten DJ. Virus maturation by budding. Microbiol Mol Biol Rev. 62: 1171-1190. 1998.

[23] Fehr AR, Perlman S. Coronaviruses: an overview of their replication and pathogenesis. Methods Mol Biol. 1282: 1-23. 2015.

[24] Wang Y, Grunewald M, Perlman S. Coronaviruses: An updated overview of their replication and pathogenesis. Methods Mol Biol. 2203: 1-29. 2020

[25] Beniac DR, Andonov A, Grudeski E, Booth TF. Architecture of the SARS coronavirus prefusion spike. Nat Struct Mol Biol. 13: 751-2. 2006

[26] Collins AR, Knobler RL, Powell H, Buchmeier MJ. Monoclonal antibodies to murine hepatitis virus-4 (strain JHM) define the viral glycoprotein responsible for attachment and cell-cell fusion. Virology. 119: 358-71. 1982

[27] Armstrong J, Niemann H, Smeekens S, Rottier P, Warren G. Sequence, and topology of a model intracellular membrane protein, E1 glycoprotein, from a coronavirus. Nature. 308: 751-2. 1984

[28] Godet M, L'Haridon R, Vautherot JF, Laude H. TGEV coronavirus ORF4 encodes a membrane protein that is incorporated into virions. Virology. 188: 666-75. 1992

[29] DeDiego ML, Alvarez E, Almazán F, Rejas MT, Lamirande E, Roberts A, Shieh WJ, Zaki SR, Subbarao K, Enjuanes L. A severe acute respiratory syndrome coronavirus that lacks the E gene is attenuated in vitro and in vivo. J Virol. 81: 1701-13. 2007

[30] Ruch TR, Machamer CE. The hydrophobic domain of infectious bronchitis virus E protein alters the host secretory pathway and is important for release of infectious virus. J Virol. 85: 675-85. 2011

[31] Westerbeck JW, Machamer CE. A Coronavirus E Protein Is Present in Two Distinct Pools with Different Effects on Assembly and the Secretory Pathway. J Virol.89: 9313-23. 2015.

[32] Chang CK, Sue SC, et al., Modular organization of SARS coronavirus nucleocapsid protein. J Biomed Sci.13: 59-72. 2006

[33] Klausegger A, et al., Identification of a coronavirus hemagglutinin-esterase with a substrate specificity different from those of influenza C virus and bovine coronavirus. J Virol. 73: 3737-43. 1999

[34] Cornelissen LA, Wierda CM, et al., Hemagglutinin-esterase, a novel structural protein of torovirus. J Virol. 71: 5277-86. 1997

[35] Hoffmann M, Kleine-Weber H, et al., SARS-CoV-2 Cell entry depends on ACE2 and TMPRSS2 and is blocked by a clinically proven protease inhibitor. Cell. 181: 271-280. 2020

[36] Bergmann CC, Lane TE, Stohlman SA. Coronavirus infection of the central nervous system: host-virus stand-off. Nat Rev Microbiol. 4: 121-32. 2006

[37] Sawicki SG, Sawicki DL, Siddell SG. A contemporary view of coronavirus transcription. J Virol. 81: 20-9. 2007

[38] de Haan CA, Rottier PJ. Molecular interactions in the assembly of coronaviruses. Adv Virus Res. 64: 165-230. 2005.

[39] Tooze J, Tooze S, Warren G. Replication of coronavirus MHV-A59 in sac- cells: determination of the first site of budding of progeny virions. Eur J Cell Biol. 33: 281-93. 1984

[40] Saraste J, Kuismanen E. Pre- and post-Golgi vacuoles operate in the transport of Semliki Forest virus membrane glycoproteins to the cell surface. Cell. 38: 535-49.1984

[41] Saraste J, Marie M. Intermediate compartment (IC): from pre-Golgi vacuoles to a semi-autonomous membrane system. Histochem. Cell Biol. 150: 407-430. 2018

[42] Klaus JP, Eisenhauer P, et al., The intracellular cargo receptor ERGIC-53 is required for the production of infectious arenavirus, coronavirus, and filovirus particles. Cell Host Microbe. 14: 522-34. 2013

[43] Machamer CE, Rose JK. A specific transmembrane domain of a coronavirus El

glycoprotein is required for its retention in the Golgi region. J Cell Biol.105: 1205-14. 1987

[44]   Machamer CE, Mentone SA, Rose JK, Farquhar MG. The E1 glycoprotein of an avian coronavirus is targeted to the cis Golgi complex. Proc Natl Acad Sci USA. 87: 6944-8. 1990

[45]   Brenda G. Hogue, Carolyn E. Machamer "Coronavirus structural proteins and virus assembly," E. . Edited by Perlman. S.; Gallagher, T.; Snijder, Ed. Washington, DC, pp. 179–200. 2008

[46]   Van der Hoek L, Pyrc K, et al., Identification of a new human coronavirus. Nat Med. 10: 368-73. 2004

[47]   Sharma A, Tiwari S, Deb MK, Marty JL. Severe acute respiratory syndrome coronavirus-2 (SARS-CoV-2): a global pandemic and treatment strategies. Int J Antimicrob Agents. 56: 106054. 2020.

[48]   Wolf YI, Kazlauskas D, Iranzo J, Lucía-Sanz A, Kuhn JH, Krupovic M, Dolja VV, Koonin EV. Origins and Evolution of the Global RNA Virome. mBio. 9: e02329-18. 2018

[49]   Zhou P, Yang XL, et al., Addendum: A pneumonia outbreak associated with a new coronavirus of probable bat origin. Nature. 588: E6. 2020

[50]   Chen B, Tian EK, et al., Overview of lethal human coronaviruses. Signal Transduction and Targeted Therapy. 5: 89. 2020

[51]   Zhong NS, Zheng BJ, et al., Epidemiology and cause of severe acute respiratory syndrome (SARS) in Guangdong, People's Republic of China, in February 2003. 362: 1353-8. 2003

[52]   Van Boheemen S, de Graaf M, et al., Genomic characterization of a newly discovered coronavirus associated with acute respiratory distress syndrome in humans. mBio. 3: e00473-12. 2012

[53]   Xia S, Liu Q, Wang Q, Sun Z, Su S, Du L, Ying T, Lu L, Jiang S. Middle East respiratory syndrome coronavirus (MERS-CoV) entry inhibitors targeting spike protein. Virus Res. 194: 200-10. 2014.

[54]   Pushkarsky, T. et al. CD147 facilitates HIV-1 infection by interacting with virus-associated cyclophilin A. Proc. Natl Acad. Sci. USA 11: 6360–6365. 2001.

[55]   He J, Tao H, Yan Y, Huang SY, Xiao Y. Molecular mechanism of evolution and human infection with SARS-CoV-2. Viruses. 12: 428. 2020

[56]   Boltz DA, Nakai M, Bahra JM. Avian infectious bronchitis virus: a possible cause of

reduced fertility in the rooster. Avian Dis. 48: 909-15. 2004

[57]   Ennaji Y, Khataby K, Ennaji MM. Infectious bronchitis virus in poultry: Molecular epidemiology and factors leading to the emergence and reemergence of novel strains of infectious bronchitis virus. Emerging and Reemerging Viral Pathogens. 13: 31-44, 2020.

[58]   Cavanagh, D. Coronaviridae: a review of corona- and toroviruses. Coronaviruses with special emphasis on first insights concerning SARS. 2005, 1-54.

[59]   Enjuanes L, Almazán F, Sola I, Zuñiga S. Biochemical aspects of coronavirus replication and virus-host interaction. Annu. Rev Microbiol. 60: 211-30. 2006

[60]   Lodish E.A. H, Berk A, Zipursky SL, "Overview of the Secretory Pathway.," Mol. Cell Biol., 2000

[61]   Cooper GM. The Cell: A molecular approach. 2nd edition. Sunderland (MA): Sinauer Associates; The endoplasmic reticulum, 2000.

[62]   Popoff V, Adolf F, Brügger B, Wieland F. COPI budding within the Golgi stack. Cold Spring Harb Perspect Biol. 3:a005231. 2011

[63]   Nakano A, Luini A. Passage through the Golgi. Curr. Opin. Cell Biol. 22: 471-8. 2010

[64]   Voss S, Li F, Rätz A, Röger M, Wu YW. Spatial cycling of Rab GTPase, driven by the GTPase cycle, controls Rab's subcellular distribution. Biochemistry. 58: 276-285. 2019.

[65]   Sannerud R, Marie M, Nizak C, Dale HA, Pernet-Gallay K, Perez F, Goud B, and Saraste J. Rab1 defines a novel pathway connecting the pre-Golgi intermediate compartment with the cell periphery. Mol Biol Cell. 17: 1514-26. 2006

[66]   Marie M, Dale HA, Sannerud R, Saraste J. The function of the intermediate compartment in pre-Golgi trafficking involves its stable connection with the centrosome. Mol Biol Cell. 20: 4458-70. 2009.

[67]   Balch WE, McCaffery JM, Plutner H, Farquhar MG. Vesicular stomatitis virus glycoprotein is sorted and concentrated during export from the endoplasmic reticulum. Cell. 76: 841-52, 1994.

[68]   Ying M, Flatmark T, Saraste J. The p58-positive pre-Golgi intermediates consist of distinct subpopulations of particles that show differential binding of COPI and COPII coats and contain vacuolar H^+-ATPase. J Cell Sci. 113: 3623-38, 2000

[69]   Klumperman J, Locker JK, Meijer A, Horzinek MC, Geuze HJ, Rottier PJ. Coronavirus M proteins accumulate in the Golgi complex beyond the site of virion budding. J Virol. 68: 6523-34, 1994.

[70]   Behnia R, Munro S. Organelle identity and the signposts for membrane traffic. Nature, 438: 597-604, 2005.

[71]   Nickel W, Rabouille C. Mechanisms of regulated unconventional protein secretion. Nat. Rev. Mol. Cell Biol. 10: 148-55, 2009.

[72]   Pompa A, De Marchis F, Pallotta MT, et al. Unconventional Transport Routes of Soluble and Membrane Proteins and Their Role in Developmental Biology. Int J Mol Sci. 18: 703, 2017.

[73]   Grieve AG, Rabouille C. Golgi bypass: skirting around the heart of classical secretion. Cold Spring Harb Perspect Biol. 3:a005298, 2011

[74]   Ahat E, Li J, Wang Y. New Insights Into the Golgi Stacking Proteins. Front Cell Dev. Biol. 7: 131, 2019.

[75]   Lane JD, Lucocq J, Pryde J, Barr FA, Woodman PG, Allan VJ, Lowe M. Caspase-mediated cleavage of the stacking protein GRASP65 is required for Golgi fragmentation during apoptosis. J Cell Biol. 156: 495-509, 2002

[76]   Rabouille C, Kondylis V. Golgi ribbon unlinking: an organelle based G2/M checkpoint. Cell Cycle. 6: 2723-9, 2007

[77]   Kuo A, Zhong C, Lane WS, Derynck R. Transmembrane transforming growth factor-alpha tethers to the PDZ domain-containing, Golgi membrane-associated protein p59/GRASP55. EMBO J. 19: 6427-39, 2000

[78]   Desmyter W. E. R. J, Melnick J L, "Defectiveness of interferon production and of rubella virus interference in a line of African green monkey kidney cells (Vero)," J. Virol., 1968.

[79]   Klausner RD, Donaldson JG, Lippincott-Schwartz J. Brefeldin A: insights into the control of membrane traffic and organelle structure. J Cell Biol. 116: 1071-80, 1992.

[80]   Saraste J, Svensson K. Distribution of the intermediate elements operating in ER to Golgi transport. J Cell Sci. 100: 415-30, 1991.

[81]   Ghosh S, Dellibovi-Ragheb TA, Kerviel A, et al. β-coronaviruses use lysosomes for egress instead of the biosynthetic secretory pathway. Cell. 183: 1520-1535, 2020.

[82]   Saraste, J. and Kuismanen, "Pathways of protein sorting and membrane traffic between the rough endoplasmic reticulum and the Golgi complex.," Semin. Cell Biol, 3: 343–355, 1992.

[83]   Saraste, J., Palade, G.E. & Farquhar, M.G. Antibodies to rat pancreas Golgi subfractions: identification of a 58-kD cis-Golgi protein, J Cell Biol, 105: 2021–2029, 1987.

[84] Hauri, H.P., Kappeler, F., Andersson, H., Appenzeller C , ERGIC-53 and traffic in the secretory pathway," J Cell Sci, 1133: 587–96, 2000.

[85] Ortiz Sandoval C, Simmen T. Rab proteins of the endoplasmic reticulum: functions and interactors. Biochem. Soc Trans. 40: 1426-32, 2012.

[86] Touchot N, Zahraoui A, Vielh E, Tavitian A., Biochemical properties of the YPT-related rab1B protein. Comparison with rab1A, FEBS Lett, 256: 79–84, 1989.

[87] Jin M, Saucan L, Farquhar MG, Palade GE, Rab1a and multiple other Rab proteins are associated with the transcytotic pathway in rat liver., J Biol Chem, 271: 30105–30113, 1996.

[88] Romero N, Dumur CI, et al., Rab1b overexpression modifies Golgi size and gene expression in HeLa cells and modulates the thyrotrophin response in thyroid cells in culture., Mol Biol Cell, 24: 617–632, 2013.

[89] Saraste J, Lahtinen U, Goud B. "Localization of the small GTP-binding protein rab1p to early compartments of the secretory pathway.," J Cell Sci, 108:1541–1552, 1995.

[90] Maxfield FR, McGraw TE. Endocytic recycling. Nat Rev Mol Cell Biol. 5: 121-32, 2004

[91] Chen W, Feng Y, Chen D, Wandinger-Ness A. Rab11 is required for trans-Golgi network-to-plasma membrane transport and a preferential target for GDP dissociation inhibitor. Mol Biol Cell. 9: 3241-57, 1998

[92] Ullrich, O., Reinsch, S., Urbé, S., Zerial, M., & Parton, R. G. (1996). Rab11 regulates recycling through the pericentriolar recycling endosome. The Journal of cell biology, 135: 913–924, 1996

[93] Terasawa K, Tomabechi Y, et al., Lysosome-associated membrane proteins-1 and -2 (LAMP-1 and LAMP-2) assemble via distinct modes. Biochem.biophys. res .commun. 479: 489-495, 2016

[94] Eskelinen EL. Roles of LAMP-1 and LAMP-2 in lysosome biogenesis and autophagy. Mol Aspects Med. 27: 495-502, 2006

[95] Almazan F, Galan C, Enjuanes L. The nucleoprotein is required for efficient coronavirus genome replication. J. Virol. 78: 12683–12688, 2004

[96] Tooze SA, Tooze J, Warren G. Site of addition of N-acetyl-galactosamine to the E1 glycoprotein of mouse hepatitis virus-A59. J Cell Biol. 106: 1475-87, 1988

[97] Machamer CE. Accommodation of large cargo within Golgi cisternae. Histochem Cell Biol. 140: 261-9, 2013

[98]   Lavi E, Wang Q, Weiss SR, Gonatas NK. Syncytia formation induced by coronavirus infection is associated with fragmentation and rearrangement of the Golgi apparatus. Virology. 1221: 325-334, 1996.

[99]   Westerbeck JW, Machamer CE. The infectious bronchitis coronavirus envelope protein alters Golgi pH to protect the spike protein and promote the release of infectious virus. J Virol.193: e00015-19, 2019

[100]   Bruce EA, Stuart A, McCaffrey MW, Digard P. Role of the Rab11 pathway in negative-strand virus assembly. Biochem Soc Trans. 40: 1409-15, 2012

[101]   Rowe RK, Suszko JW, Pekosz A. Roles for the recycling endosome, Rab8, and Rab11 in hantavirus release from epithelial cells. Virology. 382: 239-49, 2008

[102]   Ulasli M, Verheije MH, de Haan CA, Reggiori F. Qualitative and quantitative ultrastructural analysis of the membrane rearrangements induced by coronavirus. Cell Microbiol. 12: 844-61, 2010